Seismic vulnerability assessment of power transmission networks

A system thinking approach

by

Jessica Ana Maria Buriticá

B.Sc., Universidad de los Andes, 2010

A THESIS SUBMITTED IN PARTIAL FULFILLMENT OF
THE REQUIREMENTS FOR THE DEGREE OF

MASTER OF APPLIED SCIENCE

in

THE COLLEGE OF GRADUATE STUDIES

(Electrical Engineering)

THE UNIVERSITY OF BRITISH COLUMBIA

(Okanagan)

April 2013

Abstract

Electrical power transmission systems are essential to the economy and well-being of modern societies. The systems consist of power generating facilities, substations, and supervisory control and data acquisition, which are inter-connected through transmission lines arranged within a high dimensional network (i.e., large amount of edges and nodes). Efficiency and service quality are influenced by reliability of this network. Therefore, identification of critical components and vulnerability analysis become paramount, in particular, in regions where seismic activity is significant.

In this research a novel methodology for seismic vulnerability assessment of power transmission systems is developed. The analysis is carried out from the perspective of both the system's form (i.e., topological-electrical importance of elements) and system's strength (i.e., probability of failure). The form combines the electrical properties of the network (e.g., electrical distance, power flow) with the systems approach via hierarchical network decomposition. On the other hand, the strength focuses on evaluating the probability of failure by means of the physical consequences of multiple earthquakes scenarios. Therefore, the vulnerability measure presents a trade–off between *strength* and *form*. Sensitivity analysis is carried out, where the influence of each perspective (i.e., *form* and *strength*) in the vulnerability measure is exhibited.

Finally, different techniques for identification of critical components are compared with the proposed methodology. The results showed that the proposed approach exhibit features that provide a better understanding of seismic vulnerability of power systems than traditional approaches.

Preface

The seismic vulnerability measure proposed in section 4.2 has been published [1]. [Jessica A. Buriticá], Buriticá, J.A., Sánchez-Silva, M., and Tesfamariam, S. (2012) "Seismic vulnerability assessment of power transmission networks using complex-systems based methodologies" in *15th World Conference on Earthquake Engineering*, no. 3418, Lisbon, Portugal, Sept 2011. I conducted all the experiments and wrote the manuscript under the supervision of Dr. Tesfamariam and Dr. Sanchez-Silva.

A version of Chapter 4 has been submitted for publication. [Jessica A. Buriticá], Buriticá, J.A., Sánchez-Silva, M., and Tesfamariam, S. (2013) Hierarchical-based Approach to Seismic Vulnerability Assessment of Power Transmission Systems, *Submitted*. I conducted all the experiments and wrote the manuscript under the supervision of Dr. Tesfamariam and Dr. Sanchez-Silva.

Table of Contents

List of Tables

List of Figures

Acknowledgements

Above all, I would like to thank God for all the blessings received along my life.

I would like to express my deepest gratitude to my principal supervisor, Dr. Solomon Tesfamariam for his guidance and support towards this thesis. Without his strong beliefs in the Socratic method, the ideas in this thesis would not have been developed. Also, I am extremely grateful with my second supervisor, Dr. Mauricio Sánchez. His good advice, support and friendship has been invaluable on both academic and personal level.

Next, I extend my thanks to Ima and Tammeen, for initiating discussions that created an environment of knowledge and enrichment, both technical and personal. Also, to all the people that contribute with ideas and discussions on this topic. Specially, Camilo Gómez, with whom the idea of hierarchical vulnerability was initially conceived.

Most importantly, I would like to express my deepest gratitude to my family, for striving every night to make me feel at home. Their encouraging words embrace me during these years. I would also like to thank Carlos, for his sincere encouragement and patience, but most importantly, for being my best friend for the last five years. I would also like to thank Apara, a friend for life, whom company and endless discussions eased and enriched my stay in Canada. Last but not least, I would like to thank all my friends in UBC, who kindly introduce me to different cultures, languages, traditions, dances, and religions. Especially to Mariel and Fabricio for offering me a sincere friendship from the very first day of school.

The financial support from Natural Sciences and Engineering Research Council of Canada (NSERC) and the UBC Okanagan Internal Research Grant Program are greatly acknowledged.

Le dedico este trabajo a mi padre, Eddier Antonio, cuyo amor y apoyo incondicional me permitió llegar aquí

Chapter 1

Introduction

The electrical power system constitutes one of the principal lifelines in a country. The power system influences nearly all aspects of modern life, from computers and electronics to finance, cooling, and lighting. Even other lifelines rely on its proper operation such as, the water supply system, communication networks, health networks and transportation. Therefore, the development of the power system has been tightly related with the growth of societies, resulting in a large-scale and highly interconnected network. This characteristic makes the power system more vulnerable to cascading failures and high consequence events.

In Table 1.1, a summary of the largest blackouts in history is presented. From this table it can be observed that even though reliability analysis of the power system is in constant improvement, large power outages continue to happen. This statement is reinforced by the findings in [2], where the blackout size distribution in the North American grid has been found to have a power tail. Therefore, large power outages are more likely to happen than expected, as a result of a conjunction of random events. Moreover, it can be suggested that global power system dynamics may follow a self-organized criticality behaviour.

Table 1.1: Largest blackouts in history

Location	**Millions of people affected**	**Date**	**References**
India	670	30-31 July 2012	[3]
Indonesia	100	18 Aug. 2005	[4]
Brazil	97	11 Mar. 1999	[4]
Brazil, Paraguay	87	10-11 Nov. 2009	[5]
United States, Canada	55	14-15 Aug. 2003	[6]
Italy, Switzerland, Austria, Slovenia, Croatia	55	28 Sep. 2003	[4]
United States, Canada	30	9 Nov. 1965	[7]

To ensure safe, economical and reliable delivery of electricity, comprehensive transmission planning is required [8, 9]. However, today's society is consistently exposed to low probability high consequence (LPHC) events, such as earthquakes, floods, terrorist attacks and chemical plant explosions. Of these, natural hazards are the major cause of power system blackouts (around 59%) [6]. Tornadoes and ice storm hazards are ranked high as common causes due to the frequency of occurrence.

However, seismic hazard can also result in devastating losses for the power system. For ex-

ample, in 1989 Loma Prieta earthquake ($M_w = 6.9$) the direct losses estimated were \$100 million [10], in the 1994 Northridge earthquake ($M_w = 6.7$) were close to \$183 million [11]; for 1995 Kobe earthquake ($M_w = 6.8$) the total cost of damage and upgrading was \$ 1 billion, according to Kansai Electric [12]. Likewise, recent earthquakes reported damage in power systems, e.g., in 2010-2011 Christchurch earthquakes ($M_w = 7.1$-Sept 2010, $M_w = 6.3$-Feb 2011, and $M_w = 6.0$-June 2011) Orion Power Company reported repair costs of \$1.7 million, \$35 million, and \$3.5 million, respectively. The only reason why these values are small compared to previous records is that the company had recently invested \$5 million (NZD) in seismic upgrading, losses of about 2-3 times were estimated if no upgrading had been done [13]. Thus, the role of incorporation of vulnerability and risk analysis of lifelines into decision making processes should be carefully studied [14–22].

Existing studies highlight the need for robust vulnerability assessment and mitigation techniques for electrical power systems. In order to assess vulnerability, different tasks have to be completed regarding the system properties, possible hazards and consequences. According to NERC [23], a risk management process includes the following steps:

1. Identification of the elements and the consequences of their potential failure
2. Identification and analysis of vulnerabilities
3. Assessment of risk
4. Identification of countermeasures, cost and trade-off

The main contribution of this thesis focuses on the first two steps. Identification of critical elements and consequences are assessed through hierarchical decomposition of networks, including electrical and topological properties of the system. On the other hand, potential vulnerabilities of the assets are analysed using seismic hazard analysis. Finally, estimation of degree of vulnerability relative to each network component is presented with the aggregation of the two previous analyses.

1.1 Power system structure

In Figure 1.1[1] the general structure of an electrical power system is shown. It is mainly composed of three sub-systems: generation, transmission and distribution. Each of the sub-systems are explained below.

1. The generation system is shown in Figure 1.1 in black. It is composed of power plants (1) and step-up transformers (2). It represents the part of the system that generates and injects power into the system (working at $\sim$ 10 to 25 kV). The principle of generation is to take advantage of electromagnetic induction in order to convert movement into electricity. This task is carried out by power plants whose source of energy can be nuclear, hydro, wind, oil, natural gas, coil, etc. In 2009, these natural resources allowed the world power industry to generate a total of 20,053 TWh[2].

[1] Figure adapted from $http://www2.econ.iastate.edu/classes/econ458/tesfatsion/Home458team.htm$
[2] Statistic taken from OECD Factbook 2011-2012: Economic, Environmental and Social Statistics

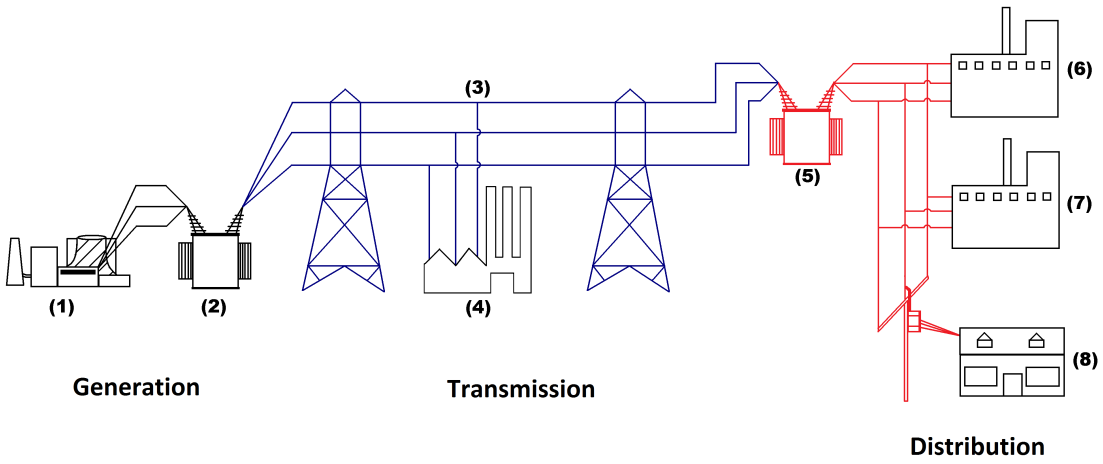

Figure 1.1: Structure of Electrical Power System

2. The transmission system corresponds to the blue section in Figure 1.1. The power transmission system consists of a group of sub–systems (e.g., power generating facilities, substations, and supervisory control and data acquisition facilities-SCADA) that are inter–connected through transmission lines (see (3) in Figure 1.1). These transmission lines operate at high voltages (138 to 800 kV) to compensate losses of electricity for conductor heating, allowing a cost-effective system for power transportation over long distances. Usually, only some large industrial users are directly connected to the transmission system (see (4) in Figure 1.1).

3. The distribution system (in red) delivers the power to final users (residential, and commercial). The distribution system usually operates below 60 or 70 kV [24], therefore a step-down transformer connects transmission and distribution, see (5) in Figure 1.1. Large commercial and industrial customers usually receive service at high voltages (4 - 13 kV), (6) and (7) in Figure 1.1, while residential users receive it at the 100-V range [3], see (8) in Figure 1.1.

A power system is usually represented using a one-line diagram, which shows all the connections and paths between power supply and users (loads). The three phases of the power system are represented by one single line. The vertical lines represent the buses (i.e., power plants or substations) and the connecting lines are the transmission lines of the system. Other elements of the system can be included such as transformers (e.g. two-winding, three-winding, potential, or current), circuit breakers (e.g., air or oil circuit breaker), and fuses. An example of a one-line diagram is shown in Figure 1.2[4]. It corresponds to a 14-node network, with 5 generation nodes and 9 load nodes. Buses with a G correspond to generation buses, and buses with a C represent synchronous compensators.

[3]The nominal value varies between networks. The nominal value in North America is 120 V.
[4]Figure adapted from [9]

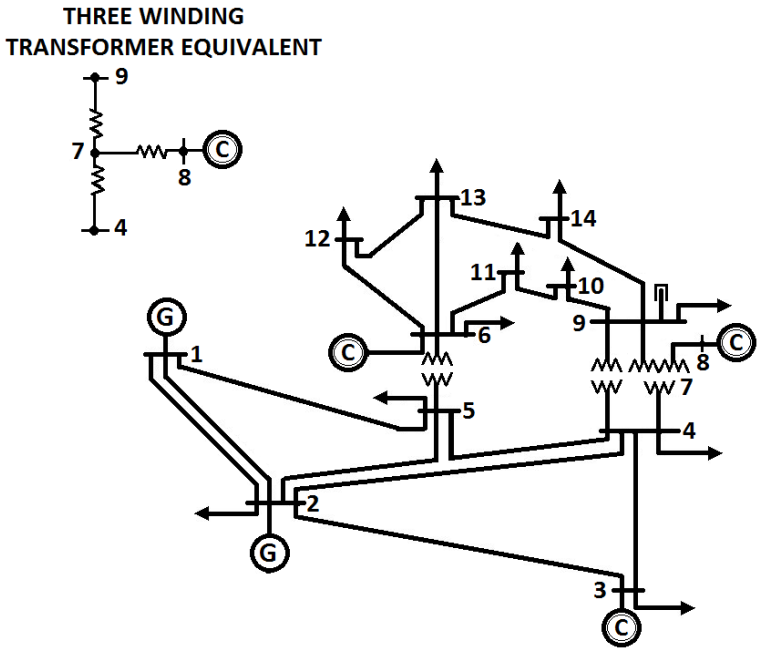

Figure 1.2: One-line diagram of IEEE Test Case with 14 buses.

1.2 Power system dynamics

The steady-state operation of an entire power system can be obtained through load flow analysis (also called power flow analysis), which tells us the current flowing through each line, the voltage and angle in each node, and direction of flow, for a specific dispatch. With this information, stability and thermal limits can be verified for system operation and management.

A power system of N nodes, can always be represented by nodal admittance or impedance matrix, which is commonly used for fault analysis [24]. If buses in the system are considered as nodes of an electric circuit, the relationship between the injected current (I) and voltage (V) can be expressed using Ohm's law $V = ZI$ (where Z is the complex impedance). However, to solve for I, the inverse of Z needs to be obtained. Moreover, in the case that two nodes are not connected to each other Z takes a value of infinity. Therefore, the admittance of the line $Y = 1/Z$ is used instead, which facilitates the computational costs. Using this representation for each node, the general equation for the power system can be defined as follows:

$$\mathbf{I} = \mathbf{YV} \tag{1.1}$$

where $\mathbf{I}$ is a vector representing the injected currents; $\mathbf{V}$ is the voltages in the nodes; and $\mathbf{Z}$ is the impedance matrix, which is the inverse of the admittance matrix $\mathbf{Y}$. The admittance matrix

$\mathbf{Y}$, is obtained as follows:

$$Y_{ij} = \begin{cases} \sum_{k=1}^{N} y_{ik} & \text{if } j = i \\ -y_{ij} = -\frac{1}{z_{ij}} & \text{if } i \neq j \text{ and line } i,j \text{ exists} \\ 0 & \text{otherwise} \end{cases} \tag{1.2}$$

where y_{ij} is the admittance of line connecting node i to node j and z_{ij} is the impedance of the lines. Note that diagonal elements represent the self-admittances, and off-diagonal elements are the mutual admittances.

Equation 1.1 give us N equations to solve. However, generation and consumption is usually given in terms of power and not in terms of current. Therefore, the relation between current and power leads us to the load flow (power flow) equations:

$$I_i = \frac{P_i - jQ_i}{V_i^*} \quad i = 1, 2, ..., N \tag{1.3}$$

where P_i, Q_i are the injected active and reactive power at node i, respectively. Subsequently, if i is a load node (i.e., it demands power), P_i and Q_i will have negative values. Incorporating this relation into equation 1.1, the N (non-linear) flow equations are found as:

$$\frac{P_i + jQ_i}{V_i} = \sum_{j=1}^{N} y_{ij}^* V_j^* \quad i = 1, 2, ..., N \tag{1.4}$$

As it can be seen, the set of equations can be split into two equations per node, corresponding to the real and the imaginary part (i.e., values of P_i and Q_i). Therefore the number of known parameters should be twice the number of equations so that the system can be solved (theoretically). As mentioned before, power consumption is usually a known parameter for a load in a power system, since it is directly obtained from the demand. Consequently, load nodes are called PQ nodes since the known parameters are: real and reactive power; and the complex voltage (i.e., V and θ) has to be found.

Similarly, generation buses are called PV nodes since real power (P) and voltage magnitude (V) are specified, and reactive power and voltage angle are unknown parameters. In fact, the generation buses can also be defined in terms of complex power; however, voltage is specified instead for convenience in balancing demanding power and operational limits [24].

Finally, the slack node (or swing bus) is the third type of node. For this particular generation bus, the known parameter is the voltage (magnitude and angle). The main reason to define this node is to have a reference for real power balance. The total amount of power in a balanced system must not only match the demanded power, but exceed it by the amount of power losses due to the resistance of the transmission lines. However, these losses are only calculated when the final value of current is obtained. Therefore, a solution to make the problem tractable is to reserve one generation bus (the slack bus) to supply only the power due to losses.

Theoretically, if the number of known parameters is equal to the number of equations, a solution should be obtained. However, the calculation of a.c. (alternating current) power flow equations does not have a closed-form solution [24]. So, iterative models are used to solve the equations: Newton-Raphson, Gauss, Gauss-Seidel and Fast Decoupled Method are most commonly used. Explanation of these models for solving power flow equations can be found in [24, 25].

For practical purposes, a d.c. (direct current) model of the system gives a close approximation to the a.c. behaviour [24]. Therefore d.c. analysis has been widely used to analyse the operation of power systems. In a power system of $N+1$ buses the d.c. power flow equations are presented as follows:

$$U_B = Z_B I_B \tag{1.5}$$

where U_B is a vector that represents the d.c. voltage in each bus (node), and I_B is the d.c. representation of the injection current. The equivalent impedance between a pair of buses is described in terms of a real part called resistance (R) and the complex part, reactance (X). The first assumption for this approach is that the line losses are ignored, which indicates that the resistance of a line is zero, and in consequence, the impedance is calculated only in terms of the reactance.

Efficiency of networks, specifically of power networks, has been studied as a measure of performance. Moreover, changes on the network efficiency after a disturbance are considered as a measure of consequence [26–28]. From the complex-systems perspective, the efficiency of a network is defined as the effectiveness of communication between a pair of nodes. This measurement is calculated as the inverse of the geodesic distance (or shortest path), since it is assumed that the communication between every pair of nodes flows through shortest paths. This is the case for some networks, such as transportation, and communications. Nevertheless, in electrical power systems, the current flows through all the lines that belong to any path in-between. Furthermore, the amount of current flowing through each line depends on the impedance of that line.

Arianos et al. [27] introduced the definition of *electrical distance* (δ_{ij}) as the cost of the energy to transit from bus i to bus j, and it is formulated in terms of the impedance of the line as:

$$\delta_{ij}^{k} = |Z_{ij}| = |z_{i,i}| + |z_{j,j}| - 2 * |z_{i,j}| \forall k \tag{1.6}$$

where k is any path, and the distance between a pair of nodes i, j is calculated in terms of the magnitude of the equivalent impedance Z_{ij} (see [27] for details). Using this definition, the efficiency is reformulated in terms of electrical distance and the power transmission capacity. The new efficiency is called net-ability, and is defined as the following global indicator [27]:

$$K = \frac{1}{N_{\mathcal{G}} N_{\mathcal{L}}} \sum_{j \in \mathcal{G}} \sum_{i \in \mathcal{L}} \frac{C_{i,j}}{Z_{i,j}} \tag{1.7}$$

where $N_{\mathcal{G}}$ is the number of generation buses, $N_{\mathcal{L}}$ is the number of load buses, and $C_{i,j}$ is the power transmission capacity between a pair of nodes. Likewise, the power transmission capacity

is defined as [29]:

$$C_{i,j} = \min_{l \in \mathcal{E}} \left(\frac{p^l_{max}}{|f^l_{ij}|} \right) \tag{1.8}$$

where p^l_{max} is the maximum power transmitted through line l, and f^l_{ij} is the change of the power on line l ($l \in \mathcal{E}$) for injection at generation bus i and withdrawal at load bus j. f^l_{ij} is obtained as the difference between the entries f_{li} and f_{lj} of the Power Transmission Distribution Factor (PTDF) matrix ($\mathbf{P}$).

1.3 Illustrative example

The IEEE-14 Test case is used to illustrate the concepts used for d.c. power flow, specifically the calculation of electrical distance and net-ability. In Figure 1.2 the one-line diagram of the system is shown. The bus data and branch data is obtained from the repository of the University of Washington [30]. Let's first define the parameters of the network:

- Swing bus is generation node # 1
- $\mathcal{G} = \{2, 3, 6, 8\}$
- $\mathcal{L} = \{4, 5, 7, 9, 10, 11, 12, 13, 14\}$
- $N_{\mathcal{L}}$=9
- $N_{\mathcal{G}}$=5
- Number of lines $N_{\mathcal{E}}$=20
- Admittance matrix $\mathbf{Y}$ is 14x14
- Impedance matrix $\mathbf{Z}$ is 13x13[5]

Once the parameters are defined, the first value to calculate is the admittance matrix, which will help us to obtain both the equivalent impedance (i.e., electrical distance) and PTDF matrix. As explained in [27], the line losses are ignored, so the line impedance Z_{ij} in equation 1.2 is only expressed in terms of the line reactance x_{ij} (see Table A.1 in Appendix A). Similarly, the line susceptance is considered to be negligible [27].

The electrical distance δ_{ij} for every pair of nodes is then obtained using equation 1.6[6]. In Table A.2 of Appendix A, the final electrical distance matrix is shown. As expected, the diagonal elements are zero and off-diagonal elements depend on the impedance between every pair of nodes. Notice that since bus # 1 is the reference node, the entry (i, j) of the matrix is actually the distances of nodes $i + 1$ and $j + 1$.

On the other hand, the power transmission capacity is defined for a pair of generation and load nodes, and depends on the line flow limits and the PTDF values (see equation 1.8). Since

[5]Notice that the swing bus is removed to reference all impedances to it

[6]Only the magnitude of $\mathbf{Z}$ is used for obtaining the electrical distance, to avoid complex values of distances

there are 5 generation nodes and 9 load nodes, there are $5 * 9 * N_{\mathcal{E}}$ values to calculate for the PTDF. As an example, the PTDFs for generation node 2 and load node 14 are shown in Table 1.2. The sign of the PTDF value indicates the direction of the power flow with respect to the reference direction (e.g., for line (1,2) the reference direction is from 1 to 2); however, the PTDF has a negative sign, indicating that the flow direction is in fact from 2 to 1. The line flow limits for the IEEE-14 Test Case are not specified in the data; for calculation purposes we will assume it to be the maximum generation value of PV nodes, which is 40 MW. For this pair of generation and load node $C_{2,14}$ is approximately 66 MW. This indicates the amount power injected at node 2 when the first line in all the lines connecting bus # 2 with bus # 14 reaches its limit.

Table 1.2: PTDFs for injection in bus 2 and withdrawal in node 14

PTDF entry	Value	PTDF entry	Value
$f_{1,2}^{2,14}$	-0.19437	$f_{6,11}^{2,14}$	0.0289
$f_{1,5}^{2,14}$	0.19437	$f_{6,12}^{2,14}$	0.0878
$f_{2,3}^{2,14}$	0.15849	$f_{6,13}^{2,14}$	0.3070
$f_{2,4}^{2,14}$	0.33168	$f_{7,8}^{2,14}$	0.0000
$f_{2,5}^{2,14}$	0.31546	$f_{7,9}^{2,14}$	0.3662
$f_{3,4}^{2,14}$	0.15849	$f_{9,10}^{2,14}$	-0.0289
$f_{4,5}^{2,14}$	-0.08618	$f_{9,14}^{2,14}$	0.6052
$f_{4,7}^{2,14}$	0.36622	$f_{10,11}^{2,14}$	-0.0289
$f_{4,9}^{2,14}$	0.21013	$f_{12,13}^{2,14}$	0.0878
$f_{5,6}^{2,14}$	0.42365	$f_{13,14}^{2,14}$	0.3948

Following the same procedure for every pair of generation and load nodes, the net-ability of the system is obtained using equation 1.7. For this network, the net-ability K is equal to 252.8, which give us a measure of the efficiency of the network[7].

1.4 Outline and scope

In this thesis a methodology for seismic vulnerability assessment is presented. The analysis is carried out from the perspective of both the system's *form* (i.e., topological-electrical importance of elements) and system's *strength* (i.e., probability of failure). The *form* combines the electrical properties of the network (e.g., electrical distance, power flow) with the systems approach via hierarchical network decomposition. On the other hand, the *strength* focuses on evaluating the probability of failure by means of the physical consequences of multiple earthquakes scenarios.

In Chapter 2, a summary of vulnerability assessment of power systems is presented; focusing on the development of vulnerability of power systems from complex systems approach. In Chapter 3, the systems approach methodology for assessing vulnerability of complex networks is explained in detail. In Chapter 4, the proposed methodology is developed: first, an introduction to seismic hazard analysis and representation is presented; second, the hierarchical seismic vulner-

[7]Notice that the units of the net-ability are $[A^2]$, which is a measure related to current flow.

ability assessment methodology is explained, combining the topological, electrical and structural characteristics of the power system; third, a case study is presented to illustrate the concept of hierarchical seismic vulnerability; and finally, a comparison study with other topological vulnerability measures is presented. In Chapter 5 a sensitivity analysis is presented for variation in the hierarchical approach, and variation in the seismic response of structures. Finally, conclusions and future work are presented in Chapter 6.

Chapter 2

Vulnerability Analysis of Power Systems

Vulnerability analysis is used in the electric industry as part of decision-making process for the identification of critical components and proper countermeasures to mitigate threats [23]. Holmgren [31] provides a thorough definition of vulnerability for engineering applications (e.g., industrial systems, road system, information security, military, and mathematics) as:

> *"The collection of properties of an infrastructure system that might weaken or limit its ability to maintain its intended function, or provide its intended services, when exposed to threats and hazards that originate both within and outside of the boundaries of the system".*

Bompard et al. [32] describes the physical behaviour of a power system in terms of: topological structure and operational state. Therefore, analysis of power systems such as vulnerability can be addressed from different perspectives, i.e., what they call "conventional" vulnerability assessment and "structural" vulnerability. The conventional vulnerability approach analyses the operational state (i.e., load flow equations) of the system before and after any disturbance and measures vulnerability in terms of the change of state. However, as mentioned in Chapter 1, this is a demanding task that requires iterative process, which might not be suitable for practical applications and some decision-making process. On the other hand, power flow dynamics is highly dependant on the topological structure of the system, so a less computational demanding, though representative, methodology for vulnerability assessment can use topological analysis of power systems [32].

Additional to this classification, a third kind of vulnerability assessment techniques has been reported, using probability representation of power system components and behaviour. Hence, we classify the vulnerability techniques into: 1) probability-based [8, 20, 33–35]; 2) complex-system theory based (topological approach) [29, 36–39]; and 3) physics-based models (conventional approach) [40–44].

In general, from the electrical engineering perspective, vulnerability analysis of power systems focuses on analysing the response of the system to random or intentional attacks [42]. In other words, few approaches implement analysis of specific hazard, like seismic hazards [45]. Moreover, it seems that the literature for seismic vulnerability analysis is developed separately by earthquake and civil engineers. Shinozuka et al. [46] pointed out the complexity of seismic vulnerability analysis task and highlighted the importance of integration of disciplines of civil,

mechanical, electrical engineering and seismology. Aimed by this, our principal goal is to propose a novel methodology for seismic vulnerability assessment of power systems. This methodology should integrate knowledge of vulnerability analysis (specifically from topological approach) with seismic hazard analysis.

In the following sections, a brief review of current vulnerability analysis techniques is presented, including advantages and disadvantages for decision-making. Detailed development of "structural" vulnerability is also included. Moreover, a section on seismic vulnerability from earthquake engineering perspective is presented.

2.1 Probabilistic-based methods

In probability-based methods, the probability theory is used to extract the behaviour of the system, the characteristics of the elements and disturbances behaviour, the latter is common in almost all the vulnerability analysis approaches. In these approaches, the elements that characterized the system (load demand, voltage, power flow, etc.) are considered to be random variables and they are represented by their probability distribution function, which can be extracted from historical data, expert knowledge, or literature. Once the system behaviour is obtained, the disturbance is simulated as a random variable, and the consequences in the system are analysed in order to calculate the vulnerability of the system. In this particular view, the vulnerability is measured in terms of the probability of system failure.

Depending on the approach, two major techniques for measuring the impact on the system could be used: the probabilistic approach or the analytical approach [34]. The probabilistic approach performs a great amount of simulations in order to obtain a representative vulnerability measures samples and calculate the probability distributions (e.g., [20]); and the analytical approach, uses mathematical models and its solutions to make the probability calculations [34].

The major advantage about probabilistic techniques is that the complexity of the system behaviour can be integrated in a set of distributions. Moreover, the information of the grid is included in the vulnerability analysis, regardless of the power flow. Although it is true that some uncertainties exist in the power flow of an electrical system, for a lot of decision-making processes, only the limits of the system and the minimum level of vulnerability are required. In this sense, an exhaustive analysis of the system could be unnecessary, but only the worst case (e.g., in the flow of the power system), as well as different contingency cases, should be considered.

2.2 Physics-based methods

The principal characteristic of the energy-function method is that vulnerability is measured by using the energy function of the power grid. Approaches in this field define the vulnerability of the system as a combination between the current vulnerability (difference between current energy and energy in stable state) and a measure of the trend of the system to change its current state to a vulnerable state. Furthermore, in these approaches, the disturbance is simulated directly

as the effect on the power flow of the system. In other words, no physical damage or failure is simulated, but only the consequences that any type of damage may raised in the electrical dynamics (e.g., high energy flow between lines). Some techniques used for the calculation of the energy function are Transient Energy Function (TEF) [40, 43] and Branch Potential Energy model (BPE) [44].

Techniques based in energy function implement pure electrical analysis for the system vulnerability measurement. The advantages of these techniques are that the electrical properties and electrical dynamics of the system are captured, i.e., a realistic simulation of the system is performed. Moreover, on-line calculations can be done. On the other hand, the system is not considered as a whole, but only focused on each particular component, which might ignore the dynamics (not electrical, but interdependencies) and intrinsic properties of the power systems. For this reason, these techniques are not the best alternative for the seismic vulnerability analysis, because the high-level disruption of the system and different levels of impact cannot be easily included and interdependencies between elements are ignored.

2.3 Complex-systems-based methods

Vulnerability in terms of complex system theory, is the study of the topological changes (e.g., degree distribution, betweenness centrality), subject to a disturbance in the system [47]. Disturbances are simulated by removing nodes. This deletion process can be executed randomly or systematically, which can cause different levels of consequences (e.g., very large, moderate, minor), depending on the model of system (e.g., scale-free, random, small-world) that is being analysed.

Electrical power systems were initially modelled as complex systems by Watts and Strogatz [36], where the topological properties classify the U.S. power grid as "small-world" network. However, Barabasi and Albert [37] found that as many other complex networks, the U.S. power system vertex connectivities follow a scale-free power law distribution. This is later identified to be an indication of its vulnerability, when power outages seem to follow the same power law [2]. Similar studies are developed for the Italian grid [47] and the complete European grid [39].

Identification of critical components and vulnerability analysis is initially addressed using topological analysis [31, 38, 48, 49]. Simultaneously, other approaches incorporate the topological analysis (i.e., complex-system theory) into a process of successive clustering, with the aim of extract intrinsic properties of the network (e.g., electrical properties) and detect vulnerabilities into communities of the network [50]. However, conventional definitions of topological measures, failed to represent the power flow dynamics of the system[8]. Therefore, new approaches [27–29, 32, 51] address the identification of critical elements and vulnerability re-defining topological concepts such as distance, betweenness, and efficiency using electrical information of the system.

The main disadvantage of complex-systems approaches is that they do not include power flow

[8]This is due to the fact that current flows through all possible paths and not just shortest paths

representation of the power system in the vulnerability analysis [52]. Consequently, results are less reliable compared to other techniques. However, with the introduction of the new concepts of efficiency and electrical distance that have been recently proposed, this is no longer a problem. However, it is important to mention that topological analysis (even enhanced) does not replace the conventional approach, but serves as a complementary tool that can be used in decision-making process that do not require full operational analysis [32]. Additionally, complex theory includes the vulnerability analysis of internal properties of the network dynamics and interdependencies that cannot be easily included using other techniques.

2.4 Seismic vulnerability

Construction of infrastructure systems has always been based on building codes and manuals that strive to ensure safety and reliability. However, with the development of engineering tools and software, new modelling techniques are feasible and more realistic simulations have resulted in release of new construction manuals and codes. Seismic analysis for power systems have followed a similar trend. The amount of data gathered from past earthquakes has been used to develop probabilistic models to analyse seismic response of power systems, this approach is called probabilistic seismic hazard analysis (PSHA). On the other hand, recent software tools provide enough computational capacity to develop scenario based simulations with realistic performance analysis [53]. Therefore, depending on how the seismic hazard is modelled, performance evaluation can be either deterministic or probabilistic. Each of these approaches has its advantages and drawbacks, which have been previously explored (see [53]).

PSHA describes the seismic hazard through a probabilistic representation such cumulative distribution. This representation is obtained in terms of the effect in certain location of a set of probable seismic scenarios, weighted by how probable they are. The main advantage of this approach is the consistency of the seismic hazard representation in a given region (e.g., size, attenuation, and frequencies of occurrence), which allows a consistent decision-making process, such as building design, retrofitting, demolition or resource optimization for seismic risk analysis [54]. One of the most important applications of PSHA is the creation of seismic hazard maps for different return periods for U.S., available in [55]. Moreover, they have been used in applications involving risk assessment, for example [56, 57].

The main drawback of PSHA is that fails to represent correctly the spatial distribution of seismic intensities [53], which is a key element in the study of systems whose elements are widespread, e.g., lifelines [58]. Consequently, analysis of seismic performance of power systems have been dominated by deterministic approaches, i.e., scenario-based seismic hazard representation. For example, Shinozuka et al. [59], Liu and Feng [16], and Nuti et al. [60] proposed strategies (physical or electrical) for seismic damage mitigation using power flow analysis to determine the direct and indirect consequences of the earthquake scenarios. Moreover, Schiff [15] and Knight and Kempner [61] focused in the identification of seismic vulnerabilities through physical analysis of power system elements and propose frameworks for seismic response and evaluation. Furthermore, the probabilistic approach has been implemented in seismic analysis of power systems by Adachi and

Ellingwood [62], Jun and Jie [63], and Gardini et al. [64]. Finally, complex-system theory has been explored by Duenas-Osorio et al. [65] to analyse seismic response of interdependent networks.

Scenario-based seismic analysis, is usually based on a Monte Carlo simulation where the following procedure is repeated several times:

1. Sample a possible earthquake scenario and effects (i.e., seismic action)
2. Sample component fragilities
3. Identify non-functional components and cascading effects and update the network accordingly
4. Run power flow analysis for the updated (damaged) network
5. Calculate performance index

Work has been reported to obtain the fragility of the different components of a power system [56, 66–69], including data gathering from previous earthquakes [70]. These fragilities represent the probability of exceedence of certain damage state, given a ground acceleration value[9] (from seismic scenario). Therefore, analysing the damage state of each component can lead to a new configuration of the system, in case the cascading failure is spread out of the station or even if certain substations or lines are out of service.

The main difference among approaches is in the third step of the procedure: how to determine functionality of components and cascading effects [71]. The functionality of an electrical component is usually modelled as a combination of micro-components that determine the damage state of a particular station (substation or generation node). A simple approach is to have a failure/safe assumption of the station model with no internal logic, e.g., [61, 72]. However, multi-state components are a more realistic approach and state-of-art tendency, where failure can be spread through the system. This analysis has been performed for different power systems such Italian network [64]; Los Angeles (CA) power system [46], Shelby County (TN) power network [53, 65], San Francisco (CA) power network [72] and Sicily (Italy) power network [71], among others.

Standard configurations of substations are: breaker-and-a-half, double-bus-double-breaker, double-bus-single-breaker and ring bus [10]. Differences between them rely on the configuration of the *bus*, which refers to the main conductors that connect sets of transmissions lines [10]. These configurations are used to analyse seismic performance, e.g. [10, 46, 59]. The components here analysed are basically disconnected switches, buses, circuit breakers and transformers, i.e., with no micro-components.

On the other hand, Vanzi [73] presents one of the widely cited configurations to analyse a substation [60, 64, 71, 74–77]. The substation is first divided into micro and macro-components, where performance and damage state of macro-component is fully described by damage state of

[9] This is discuss in more detail in section 4.1.2

its micro-components [73]. Macro-components identified are: 1) Lines without transformer; 2) bars-connecting line; 3) bars; 4) line boxes; 5)power supply to protection system; 6) autotransformer line and 7) switches; each of them represented by a list of micro-components (for details see [73]). In case of failure of a micro-component, the macro-component is insulated. Furthermore, the failure causes a short-circuit propagation that can lead to failure or insulation of other macro-component, depending on the behaviour of switches and protection devices.

Once the damages due to seismic hazard are calculated, power flow analysis is developed and flow limits and stability is checked in the network [60]. If any limit is exceeded, respective lines or load nodes are removed from the network. Finally, direct and indirect cost are calculated using a performance measure [59]. This measure depends on the power delivered and it can be expressed in terms of unattended power (weighted or not)[46, 60, 64, 71], connectivity drop [65], failure probability (statistical representation) [62, 78], reparation time/cost, among others.

Chapter 3

Systems Approach for Complex Networks Analysis

Systems approach, also called *systems thinking*, is a discipline mostly developed in recent years (20^{th} century) in the context of biology, ecology, psychology and cybernetics to model systems with complex interactions and structures [79]. Moreover, it has recently gained importance in operational research and management science, as a way to approach the analysis of social networks, infrastructure networks, information systems, medical and public health, and even natural environment. A complete review on contributions and applications can be found in [80]. According to Mingers and White [80], the key elements of systems approach are:

- Consider the problem (i.e., network analysis) as interacting elements in an environment.
- Interactions between elements, not individual elements are key to understand the system dynamics.
- There is an intrinsic hierarchy in the system and therefore, emergent properties and interactions between "sub-systems" and within "sub-systems".

Considering the aforementioned description, a hierarchical representation seems to be appropriate [81]. A hierarchy represents a system from its overall behaviour (top of the hierarchy) to the detailed relationships of its components (bottom of the hierarchy), facilitating the understanding process of the system performance. Furthermore, it can also be used to extract intrinsic information about the network, to enhance decision-making process and to reduce the computational costs associated with it [81].

However, usually in complex networks the interactions and interconnections between elements are such that the detection of sub-systems can become a difficult task, e.g., in power systems. Although substations and power plants have a physical location, the interactions between them are not exactly related with these physical distances. For instance, the operating state of an electrical power system is described through power flow analysis, which in turn is represented by a series of differential equations. Therefore, special algorithms are needed to find the internal structure.

In this line, clustering algorithms has been applied to identify communities of a system that share certain properties. Applications can be found in different fields such as biology, machine learning, pattern recognition, data mining, image segmentation, civil engineering, geology, economy and social sciences [82, 83]. The system thinking approach has been applied previously for

decision-making processes of infrastructure systems for resource allocation [84, 85], risk assessment [81], and project management [86].

In the following section, a brief introduction to clustering algorithms is presented. Then, in the subsequent section, the development of hierarchical decomposition by means of recursive clustering is explained, as well as concepts involved for detection of critical components.

3.1 Clustering Analysis

According to Abonyi and Feil [87] clustering is "the partitioning of a data set into subsets (clusters), so that the data in each subset (ideally) share some common trait-often proximity according to some defined distance measure". Each of these subsets can be represented by a centroid, creating *Voronoi regions*. The *Voronoi region* corresponds to the region in the data space where all points are closer to this centroid than to any other [88] (see Figure 3.1).

The clustering process highly relies on the distance representation. Some examples of the most common distance measures to calculate proximity are shown in Table 3.1[10]. One of the purposes of using clustering algorithms is to be able to reveal hidden data structures [89]. This concept can be applied to infrastructure systems, such as power systems, to extract inherent properties of the network without prior knowledge [81].

Table 3.1: Distance measures for similarity in clustering algorithms

Measure	Equation
Minkowski distance	$D_{ij} = \left(\sum_{t=1}^{d} \lvert x_{il} - x_{jl} \rvert^{1/n} \right)^{n}$
Euclidean distance	$D_{ij} = \left(\sum_{t=1}^{d} \lvert x_{il} - x_{jl} \rvert^{1/2} \right)^{2}$
City-block distance	$D_{ij} = \sum_{t=1}^{d} \lvert x_{il} - x_{jl} \rvert$
Sup distance	$D_{ij} = \max_{1 \leq l \leq d} \lvert x_{il} - x_{jl} \rvert$
Mahalanobis distance	$D_{ij} = (\mathbf{x}_i - \mathbf{x}_j)^T \mathbf{S}^{-1} (\mathbf{x}_i - \mathbf{x}_j)$
Pearson correlation	$D_{ij} = (1 - r_{ij})/2$ where $r_{ij} = \frac{\sum_{l=1}^{d} (x_{il} - \bar{x_i})(x_{jl} - \bar{x_j})}{\sqrt{\sum_{l=1}^{d} (x_{il} - \bar{x_i})^2 \sum_{l=1}^{d} (x_{jl} - \bar{x_j})}}$
Point symmetry distance	$D_{ir} = \min_{\substack{j=1,..,N \\ j \neq i}} \frac{\lVert (\mathbf{x}_i - \mathbf{x}_r) + (\mathbf{x}_j - \mathbf{x}_r) \rVert}{\lVert (\mathbf{x}_i - \mathbf{x}_r) \rVert + \lVert (\mathbf{x}_j - \mathbf{x}_r) \rVert}$
Cosine similarity	$S_{ij} = \cos \alpha = \frac{\mathbf{x}_i^T \mathbf{x}_j}{\lVert \mathbf{x}_i \rVert \lVert \mathbf{x}_j \rVert}$

[10] This table is adapted from [89]

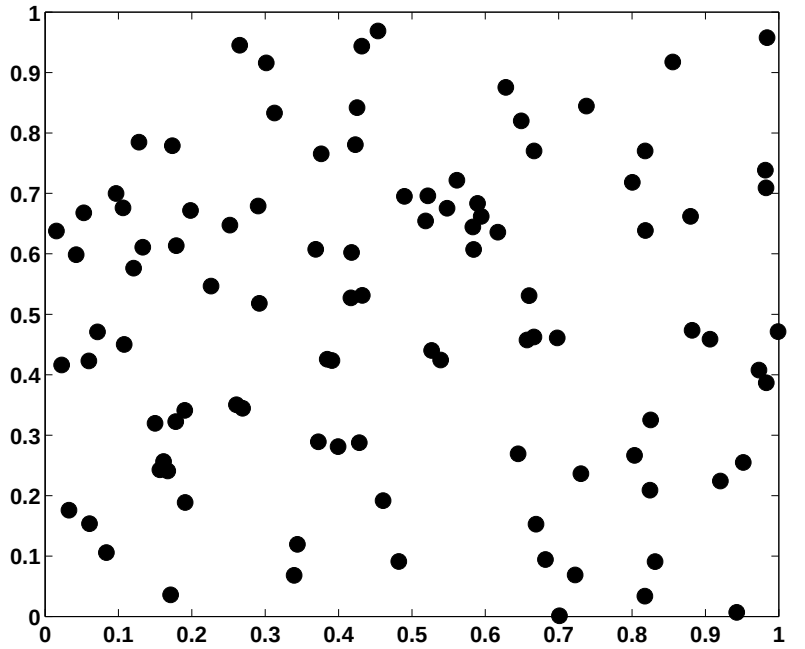

(a)

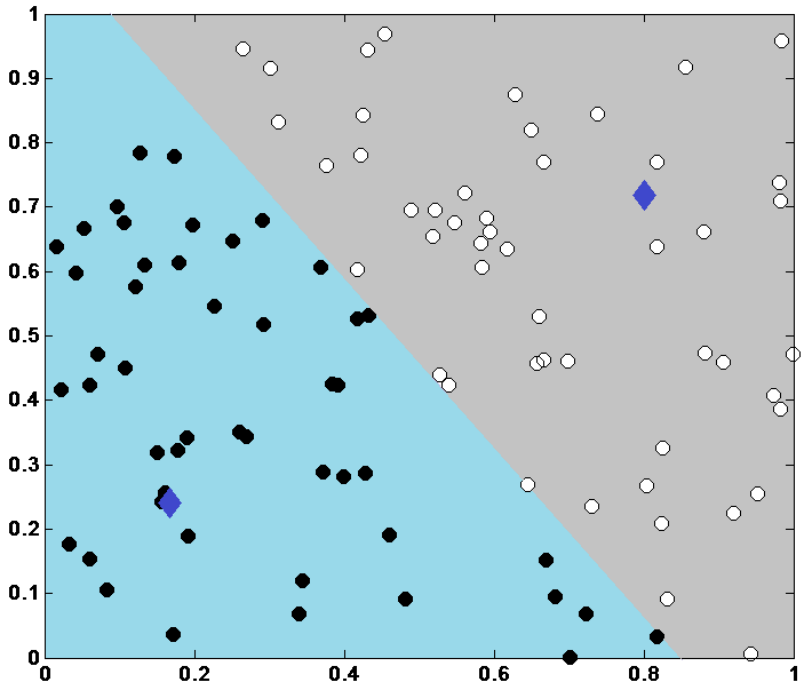

(b)

Figure 3.1: Clustering representation. a) Set of data points in 2D with its respective b) clustering representation (i.e., centroids(diamonds), Voronoi regions, and clusters)

Clustering algorithms can be classified into hierarchical and partitioning [90]. The former, recursively identify systems and corresponding sub-systems forming a hierarchical structure called

dendogram (e.g., [91],[92], and [93]). On the other hand, partitioning methods aim to find a single partition of the network, i.e., they do not seek for sub-systems within sub-systems. However, by recursively applying a clustering (any) algorithm into the clusters found, one can create a hierarchical structure.

Standard partitioning techniques (e.g. K-means, fuzzy c-means, self-organizing maps (SOM) and neural gas) fail to divide complex (non-linear) data structures [90]. But, the idea of networked world has lead to complex structures that interchange big amount of data, and the dynamics are not simple to model. Therefore, to tackle this problem spectral clustering and kernel clustering were proposed [89, 90, 94–96].

A power system can be represented by a graph, whose nodes are the substations and generation facilities, and the links are the transmission lines. However, as mentioned before, the real distance between nodes fail to represent the power flow of the network, therefore measures as *electrical distance* (see equation 1.6) are more appropriate [27]. So, the current representation has no simple partition and elaborate algorithms (e.g., spectral or kernel clustering) are needed [97].

3.2 Hierarchical Representation of Networks

Several clustering algorithms are hierarchical by nature (e.g., [91–93, 98]). However, a hierarchical representation of a network is not necessarily obtained by hierarchical clustering, in fact any clustering algorithm can be used. The aim of the hierarchical representation is to provide a compact representation of the systems dynamics for decision-making process at different levels of granularity (i.e., from general properties of the system, until properties of each element of it). The goal of clustering algorithms is to group the data in clusters that share certain information, or in other words, giving a synthetic representation of the data. Therefore, if applied recursively any clustering algorithm can produce a hierarchy with different levels of abstraction (i.e., one per recursion).

The ultimate goal of hierarchical representation of networks is to provide a structure where sub-systems at different levels of granularity are shown. Consequently, at the top of the hierarchy the agglomeration of all information of the system is presented, i.e., one single unit represent the whole network and, moreover, all the elements of the system are included in this unit. Also, it implies that the bottom of the hierarchy should represent the highest expression of granularity, i.e., each element is a "sub-system" and is represented by its particular properties. Finally, in the intermediate levels of the hierarchy, d sub-systems exists, representing clusters of elements which dynamics depend upon the shared properties of its members. Notice that the granularity of the system representation increases from top to bottom.

In order to clarify the concept of hierarchical representation, Gomez et al. [81] introduced the concept of fictitious networks. When a clustering algorithm is applied to a network, d clusters are found representing at some extent the real network. Then, these clusters can be considered as nodes of a fictitious network, whose edges are the combination of edges between the elements

that belong to each cluster. If the same clustering algorithm is applied again, but this time to the fictitious network (with its corresponding adjacency matrix), then a new level of resolution of the initial (real) network can be found, i.e., a new level of the hierarchy. If this process is performed recursively, at the end, a fictitious network with a single node is found, which contains the complete real network, i.e., the top of the hierarchy.

A formal representation of these concepts can be presented as follows [81]: At a level h of the hierarchy, a graph representation $G^{(h)}$ can be defined, where the set of vertices ($\Lambda^{(h)}$) is composed of d fictitious nodes ($\{V_1^{(h)}, V_2^{(h)}, .., V_d^{(h)}\}$, with $V_1^{(h)}, V_2^{(h)}, .., V_d^{(h)} \in V_1^1$ corresponding to clusters found at that level. Similarly, the edges between these clusters correspond to set of edges ($E^k = \{E_{1,2}^{(h)}, .., E_{d,d}^{(h)}\}$) and formed the adjacency matrix A^h.

If the original network is represented by a graph ($G_{real} = \{\mathcal{V}, \mathcal{E}\}$) of N nodes and P links, where $\mathcal{V} = v_1, ..., v_N$ and $\mathcal{E} = e_1, ..., e_P$; at the top of the hierarchy (i.e. level 1) it is found that $\Lambda^{(1)} = V_1^{(1)} = v_1, ..., v_N$. On the other hand, at the bottom of the hierarchy (level H), $\Lambda^{(H)} = \{V_1^{(H)}, V_2^{(H)}, .., V_N^{(H)}\}$, with $V_1^{(H)} = \{v_1\}$,...,$V_N^{(H)} = \{v_N\}$ (see Figure 3.2).

The previous representation of hierarchical decomposition implies a set of conceptual statements regarding the recursive clustering process [81]:

1. The clustering algorithm should provide disjoint sets of fictitious nodes (i.e., clusters) at every level of the hierarchy. Therefore, each (real) node belongs only to one cluster in each level of the hierarchy. The main reason to consider this, is that each fictitious node is considered as an independent unit [81], which represents a set of elements of the systems that share certain properties. If two clusters in the same level share a node, the independence does not hold and they can not be analysed separately.

2. The set of real nodes must be collectively exhaustive [81]. Which basically means that in each level, all real nodes must belong to a cluster. This is derived from the main objective of hierarchical decomposition: represent the whole network at different levels of resolution. If any node is excluded from the fictitious network at some level, this level does not fully represent the dynamics and properties of the original network.

3. Convexity of cluster must always hold. This implies that all the nodes in the *Voronoi region* of a cluster must belong to that cluster.

4. At any level of the hierarchy, the edge-connectivity of the fictitious network (i.e., $G^{(h)}$) has to be greater than zero. Thus, the fictitious network can not be composed of isolated (disconnected) clusters. Since the process starts with a connected network, the decomposition can not result in disconnection, but only connected clusters.

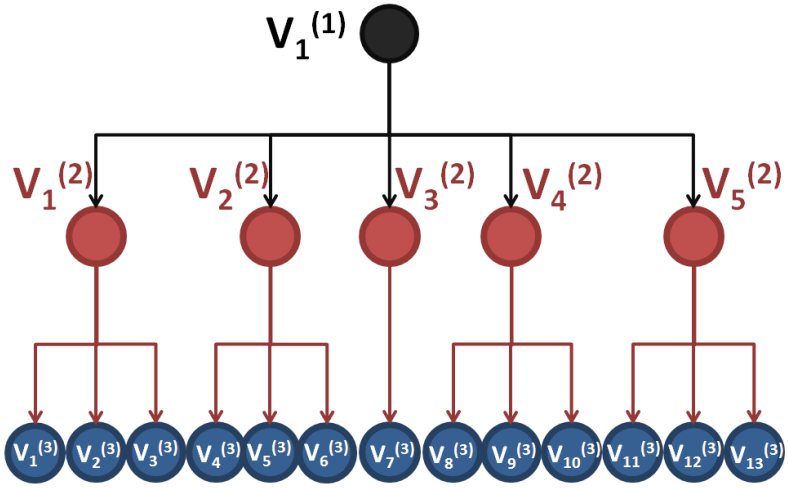

(a)

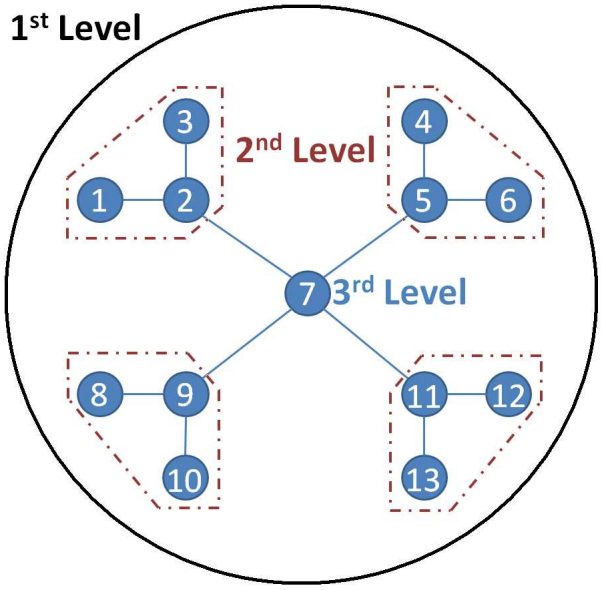

(b)

Figure 3.2: a) Hierarchical decomposition of a 13-node network and b) its corresponding fictitious networks (levels 1, 2 and 3 of hierarchy)

3.3 Illustrative example

In electrical power systems, the physical location of substations and power plants is mainly biased by the demand and geography. However, it doesn't necessarily represent the dynamics of the power flow. As mentioned in section 1.2., the power flows through all the paths between power plant and substations, therefore the typical concept for distance needs to be updated to the "electrical distance".

For the purpose of this example, the IEEE 14 Bus Test Case is used, available in [30]. In Chapter 1, in Figure 1.2 the one-line diagram was presented. As mentioned before, it consists of 14 buses: 5 power plants and 9 substations or load buses. The graph representation of such system is shown in Figure 3.3. For this representation the geographical locations are ignored, since the distance matrix is obtained from the electrical distance.

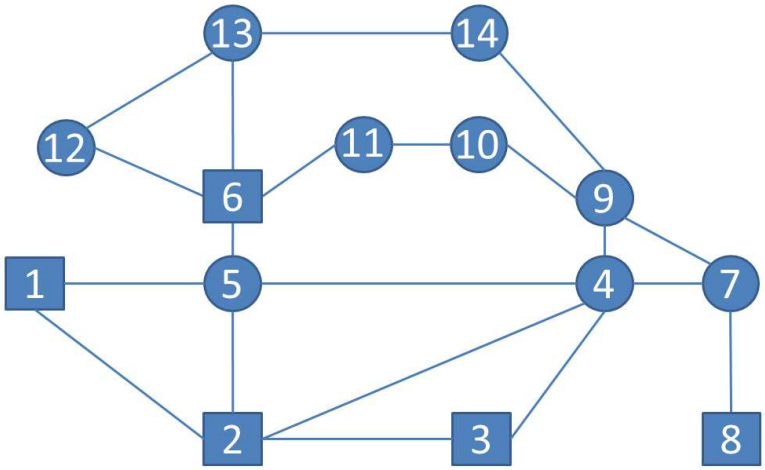

Figure 3.3: Graph representation of IEEE-14 bus Test Case

One of the most common algorithms of spectral clustering is the one proposed by Shi and Malik [98] (SM). For this illustrative example, we used SM clustering algorithm to obtain the hierarchy (this algorithm is described in detail in Chapter 4). The similarity matrix is calculated as [98]:

$$S_{ij} = \frac{-d_{ij}}{\sigma^2} \tag{3.1}$$

where d_{ij} is the distance between node i and node j; and σ^2 is a measure of data variation. In [98] σ^2 is set to be around 10% of maximum value of distance.

The electrical distance δ_{ij} calculated in previous section for the IEEE-14 Test Case (see Table A.2) is used to obtain the similarity matrix. The SM algorithm is applied recursively, assuming a binary partition in every level of the hierarchy.[11] The hierarchy is composed of four different levels as shown in Figure 3.4.

[11]The hierarchical structure obtained by SM is ignored in this example, since it is inspired to obtain a final k-partition. Thus, in every level, the previous two clusters are analysed separately and grouped, as opposite to the normal recursion of SM where only one of the clusters is selected to be divided

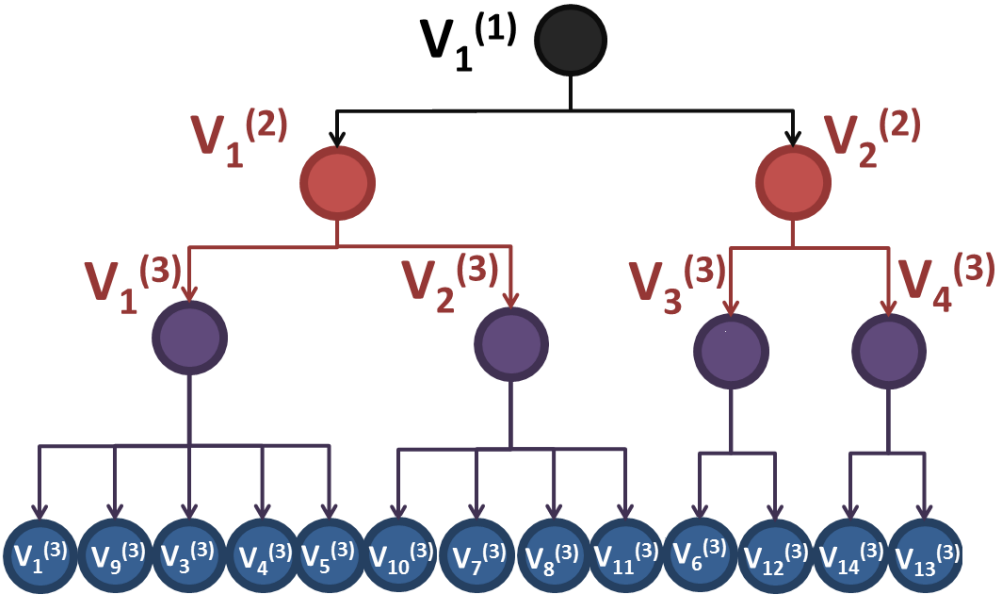

Figure 3.4: Hierarchical representation of the IEEE-14 bus Test Case

The corresponding clusters and fictitious networks are shown in Figures 3.5 and 3.6, respectively. In Figure 3.5(a), the second level of the hierarchy is shown. The first fictitious node is composed of nine (real) nodes $V_1^{(2)} = \{v_1, v_3, v_4, v_5, v_7, v_8, v_9, v_{10}, v_{11}\}$, while the second one is composed of four (real) nodes $V_2^{(2)} = \{v_6, v_{12}, v_{13}, v_{14}\}$. As shown in Figure 3.6, the fictitious network at level 2 is composed of only two nodes, representing the two clusters, where the edge between them is defined as $cut(V_1^{(2)}, V_2^{(2)})$. At this level of granularity general information regarding the power transfer between the clusters can be analysed, which may be useful for reliability and failure analysis of the power system.

Continuing with the next level in the hierarchy, in Figure 3.5(b) clustering process of third level is shown. It is evident that the clusters are not exactly biased by the location of the elements, but instead it is biased by the equivalent impedance. At this granularity level, only three fictitious nodes will be able to supply the demanded power, since node $V_4^{(3)}$ has no power plant. Therefore, analysis at this level can be useful for system recovery prioritization.

Finally, in the last level we will have 13 clusters, corresponding to the 13 nodes in the network, which is the highest level of granularity possible. Notice that node 2 of the real network is been removed from the analysis, since it is the swing bus and all the values are referred to that node.

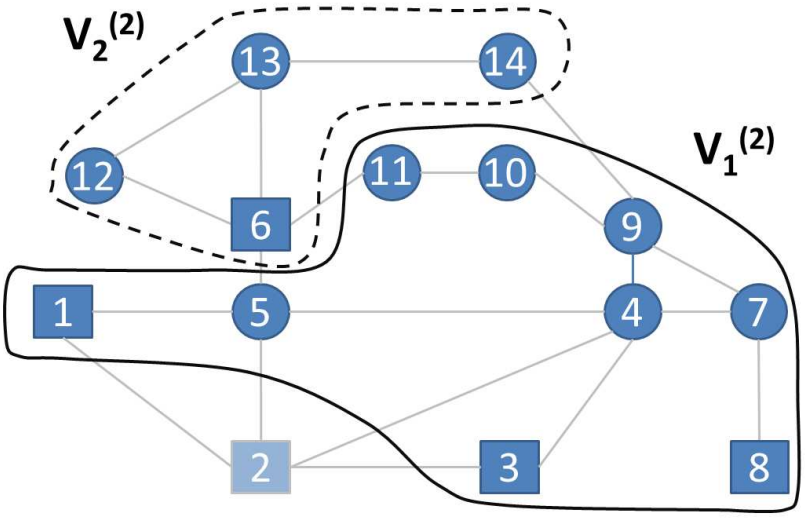

(a)

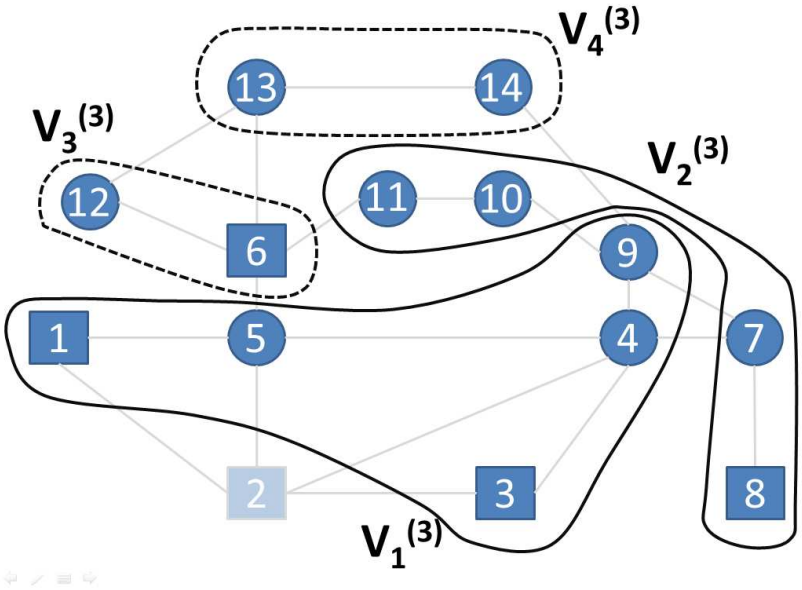

(b)

Figure 3.5: a) Clustering process at second level and b) third level of the hierarchy

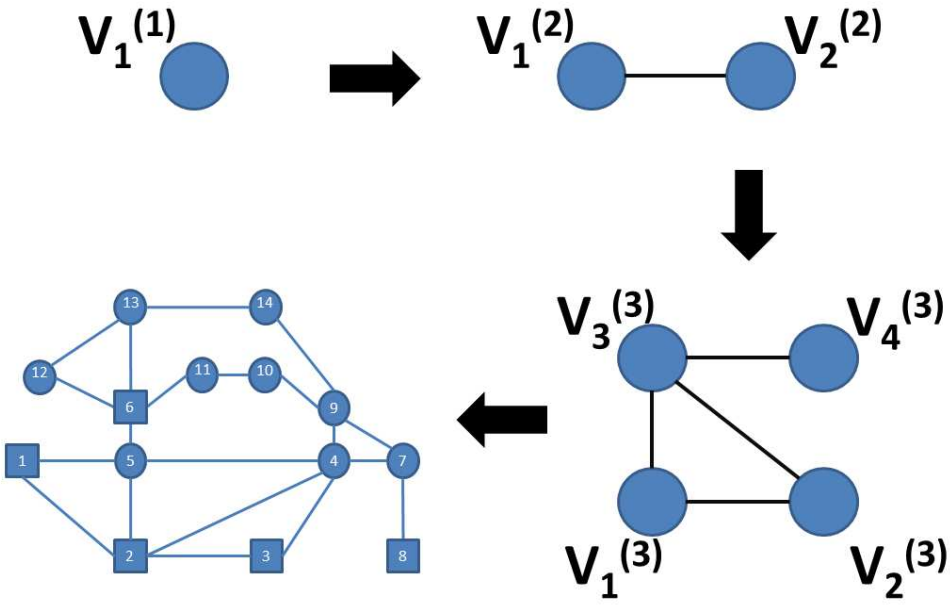

Figure 3.6: Fictitious networks for each level of the hierarchy

Chapter 4

Hierarchical Seismic Vulnerability of Power Systems[12]

Previously, identification of critical elements for vulnerability analysis in complex systems has been addressed through hierarchical decomposition. However, clustering algorithms are highly dependant on the data representation and characteristics included [90]. Depending on the complexity of the system, there are certain properties of the elements that are not easily incorporated into system data representation. In a power system, power flow dynamics and vulnerability of an element to seismic hazard are examples of such properties.

In this chapter, seismic vulnerability assessment for power systems is proposed, based on hierarchical decomposition of networks. Potential vulnerabilities of the assets are analysed with consideration of seismic hazard analysis and fragility curves (see section 4.1). Similarly, specific (electrical) measures are used to enhance the consequence analysis in order to include the power flow representation of the system.

In the following sections the implemented methodology is explained in detail, as well as each of the analysis used for obtaining the seismic vulnerability. In section 4.1, the seismic hazard representation and seismic response of power systems is explained. In section 4.2, the hierarchical seismic vulnerability measure is presented, where electrical properties are incorporated. Finally, in section 4.3, IEEE-118 network is used as case study and the results summary from this implementation is presented.

4.1 Seismic hazard and vulnerability

4.1.1 Seismic hazard representation

In order to characterize an earthquake two main elements are needed: earthquake source and earthquake magnitude [11]. To understand the source of earthquakes it is necessary to refer to the tectonic plates. These plates compose the solid part near the earth's surface and are slowly moving towards each other. The movement causes a stress on the edges of the plates such that, it can reach the strength of the rock resulting in a rupture and a significant release of energy. The rupture is called *fault* and the energy released creates what is called seismic waves [11]. The *epicentre* is the location on earth's surface above the place where the earthquake occurred.

[12]This section has been submitted for publication, see [99]

The earthquake size is the quantification of the potential damage at a location subjected to an earthquake. The most common measure to represent it is the magnitude, which can be expressed in different scales (e.g. Gutenberg-Richter, Local Magnitude, Moment Magnitude, etc.). The magnitude scale developed by Gutenberg-Richter in 1930s and 1940s is the most commonly used. In this study, the magnitude (M) can be modelled as a random variable, whose probability density function is defined as [100]:

$$P(M) = \frac{\beta e^{-\beta M}}{e^{-\beta M_{min}} - e^{-\beta M_{max}}} \tag{4.1}$$

where M_{min} and M_{max} are the minimum and maximum expected magnitude on site, and β is the severity parameter.

After the seismic source is characterized (i.e. *epicentre* and magnitude), the effect of the seismic waves at the desired location should be quantified. This energy gets attenuated as it moves far from the source through the ground. The general form for the attenuation law, relating distance from the epicentre and earthquake magnitude is as follows [101]:

$$PGA = h(M, r) = b_1(r)e^{b_2 M} \tag{4.2}$$

where PGA is the peak ground acceleration, b_2 is 0.573, r is the distance from the site to the earthquake epicentre, and $b_1(r)$ is a function of distance describing the energy dissipation. The latter, depends in the ground characteristics of the particular location and is usually obtained through statistical analysis of previous records of ground motion. Some examples of attenuation equations for different locations can be found in [102–108].

4.1.2 Fragility curves

When a seismic source is given (magnitude and epicentre) it is possible to obtain the acceleration (i.e., PGA) in any location. However, depending on the type of structure, the consequence of this acceleration may vary. Calculation of damage state of a structure for a given ground shaking can be done deterministically, assuming certain parameters of the structure. Moreover, this calculation requires assumptions regarding the ground motion and the site conditions. All these assumptions introduce uncertainty to the structural response that is not negligible [109].

The uncertainty in seismic demand related to variation of ground conditions is addressed using *fragility curves*. These fragility curves characterize the probabilistic relation between damage state and PGA [109]. The conditional probability of exceeding a damage state (DS) given a PGA ($P(ds > DS|PGA)$), is modelled using the cumulative lognormal distribution as follows [56]:

$$P(ds > DS|PGA) = \Phi\left(\frac{\ln PGA - \lambda}{\beta}\right) \tag{4.3}$$

where $\Phi(.)$ is the cumulative distribution function of the standard normal distribution; and λ and β are the mean and standard deviation, respectively. Usually the parameters given for a fragility curve are the median m (given in g, i.e., with respect to gravity) and the standard deviation β.

Therefore the mean λ is obtained as follows [69]:

$$\lambda = \ln(m) \tag{4.4}$$

In the literature, fragilities of different macro and micro-components of the power system have been studied, e.g.,[46, 56, 71]. The relation between component failure and methodology varies among the authors. The methodologies for defining fragilities curves can be empirical, numerical or mixed (i.e., both empirical and numerical)[69]. In the empirical methods probability distributions are used to approach the fragility curves; usually normal distribution (e.g.,[70, 110, 111]), or lognormal distribution (e.g.,[46, 65, 72]) are used for this purpose. On the other hand, several numerical methods have been used, e.g., fault trees [112], FORM/SORM methods [73], optimization [71], Cornell method [113], and boolean approach [56]. Finally, recent approaches combines both empirical and numerical models to enhance the fragility curves (e.g., [114–116]).

It is important to mention that each author defines different damage levels, i.e., a fragility curve is proposed per damage state and for each analysed component. Similarly, depending on the components of the power system and its specifications, the parameters of the fragility curves change. Some authors (e.g. [56, 65]) study the substations separately depending on its voltage level, i.e., low-voltage (34.5 to 150kV), medium-voltage (150 to 350kV) and high-voltage (350kV and above). Likewise, if a substation is anchored or retrofitted, the parameters of the fragility curve change. The fragility curves defined in [56] for substations without anchorage are shown in Figure 4.1, assuming a complete damage state.

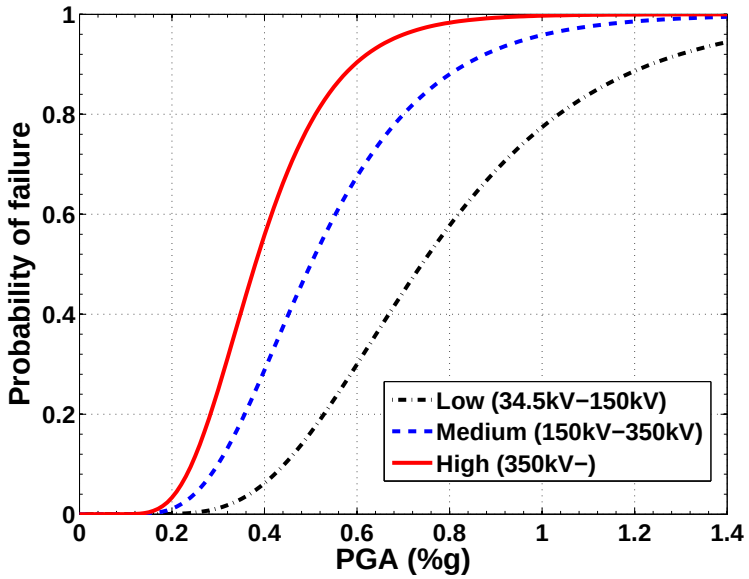

Figure 4.1: Fragility curves for complete damage of unanchored substations

Similar to substations, the generation facilities are classified according to its power generation capacity in small (less than 200MW) and medium/large (200MW and above). The corresponding

fragility curves for generation facilities from [56] are shown in Figure 4.2. In Chapter 5 the vulnerability measure for the system components is obtained using these fragility curves to analyse effect of this variation.

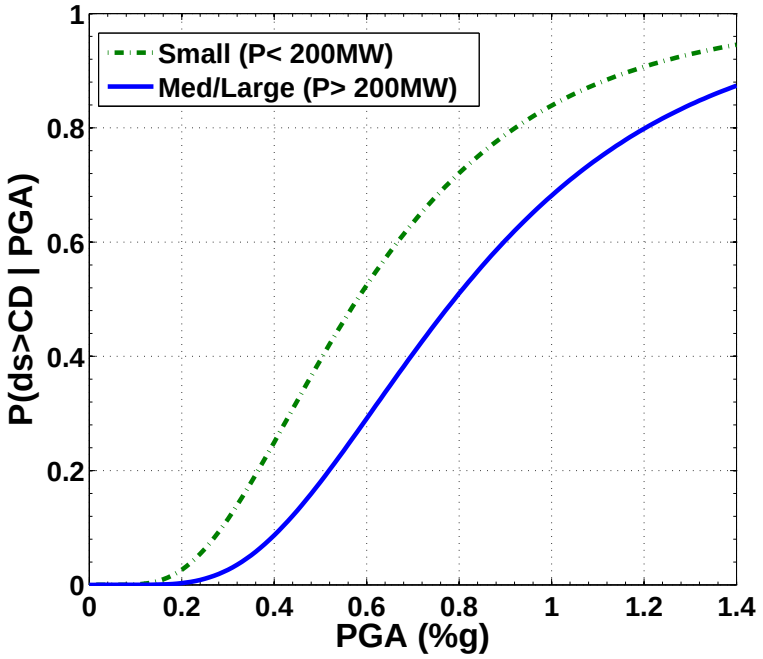

Figure 4.2: Fragility curves for complete damage of unanchored generation facilities

4.2 Seismic vulnerability measure[13]

The vulnerability measure is quantified in terms of *form* and *strength*. The system's *strength* quantifies the probability of failure to the seismic hazard for each element. On the other hand, system's *form* represents the physical (i.e., electrical) and topological importance of an element relative to the overall system's dynamics. In other words, the *form* quantifies the consequence of failure of an element of the system. Therefore, the vulnerability W is quantified in terms of system's *form* and *strength* using the hierarchical representation as follows [50]:

$$W(j) = \sum_{l in L} \mathbf{1}^{(l)}(j) c^{(l)} F(j) S(j) \tag{4.5}$$

where $W(j)$ is the vulnerability measure of element j; $\mathbf{1}_l(j)$ is an indicator function of the presence of element j as centroid of any cluster in level l of the hierarchy (see Chapter 2); $F(j)$ is the *form* factor of element j relative to the system (i.e., relative importance); $S(j)$ is the *strength* factor of element j (i.e., failure probability); and, $c^{(l)}$ is a weighting factor related to the level of resolution of the hierarchy in l (high in the top of the hierarchy and low in the bottom).

[13]This methodology was presented in the 15th World Conference on Earthquake Engineering [1]

In order to quantify values of *form* and *strength*, a specific implementation of equation 4.5 is adopted to assess vulnerability in power systems:

- The drop in net-ability ($\triangle K$ in equation 1.7 in section 1.2) is introduced as a measure of the importance (i.e., *form*) of an element in the system (see equation 4.6). In general terms, consequence can be measured in terms of change in power flow after a system disturbance. $\triangle K$ describes the change in power efficiency (i.e., change in "travel distance") after an element is removed[14]. Therefore, if a node removal causes a high drop in efficiency, this node can be considered "important" with respect to the system dynamics. Therefore, the *form* of a node is defined as:

$$F(j) = \triangle K(j) = \frac{K - K(j)}{K} \tag{4.6}$$

  where $K(j)$ is the net-ability of the network without the element j, K is the total net-ability of the network, and $\triangle K(j)$ is the drop in net–ability due to removal of node j.

  Although this measure only considers single-element failure compared to multiple failure in seismic hazard analysis, it provides an approximate quantification of consequence that can be used for long term decision-making process [29].

- The measure of the *strength* of an element ($S(j)$) is evaluated for different earthquakes scenarios through probability of failure from fragility curves, as explained in section 3.1. This work is focused on giving a general estimation of the vulnerability of the system, thus a Monte Carlo simulation is utilized for obtaining a measure for a representative number of earthquakes scenarios. Consequently, the vulnerability is calculated for each iteration and the vulnerability of each element is calculated as the mean value. Finally, a vulnerability curve is presented, representing the distribution of vulnerability measures of system's elements. In each iteration, the *strength* is calculated as:

$$S^t(j) = P(ds > CD | PGA_t(j)) \tag{4.7}$$

  where $PGA_t(j)$ is the resulting PGA in the location of element j, for earthquake scenario t; ds is the damage state and CD is complete damage.

The assessment methodology for power transmission networks using hierarchical decomposition is as follows (see algorithm 1):

1. Represent the power network by a graph G. The buses of the power system are the nodes ($\mathcal{V}$) of the graph, where the substations are denoted by $\mathcal{L}$ and the power plants are represented by $\mathcal{G}$, i.e., $\mathcal{V} = \{\mathcal{L}, \mathcal{G}\}$. The edges of the graph ($\mathcal{E}$) are the corresponding transmission lines that connect the buses.

2. Calculate the electrical distance δ_{ij} of every pair of nodes (see equation 1.6). The similarity matrix is calculated as shown in section 2.2 (see equation 3.1).

[14] In [27] the drop in net-ability is obtained for edge-removal. In this work, the node-removal is assumed to cause the disconnection of all incident edges

3. The spectral clustering algorithm is applied to the network recursively. As explained in the previous section, the entire network is represented by one fictitious node at the top of the hierarchy (see "1st level" of Figure 3.2). Every new level consists of "d" hierarchical nodes ($\mathcal{V}^{(2)} = \{V_1^{(2)}, V_2^{(2)}, ..., V_d^{(2)}\}$). This procedure is repeated to each sub–system until the real network is obtained. This implies that in the last level of the hierarchy (level l) each network node is represented by a hierarchy node, i.e., N nodes in the bottom of the hierarchy.

4. The *form* of each node is calculated in terms of the drop in net-ability ($\triangle K$) according to equation 4.6.

5. The *strength* is calculated by Monte Carlo simulation. Several hazard scenarios are developed. Each seismic scenario corresponds to a randomly generated magnitude and location of the earthquake source. Then, using the attenuation equation a PGA value is obtained in each location (equation 4.2). Finally, using the corresponding fragility curves (i.e., substations or generation facility), the probability of failure is obtained (see equation 4.3 and 4.7).

6. The vulnerability measure is quantified for each scenario as described in equation 4.5.

Algorithm 1 Seismic vulnerability analysis using hierarchical decomposition

1: $G = \{\mathcal{V}, \mathcal{E}\}$, where $\mathcal{V} = \{\mathcal{L}, \mathcal{G}\}$
2: Calculate δ_{ij} $\forall \{i, j\} \in \mathcal{V}$
3: Obtain H =recursiveClustering(G, δ_{ij})
4: Calculate $F(j)$ for all $j \in \mathcal{V}$
5: Calculate $\mathbf{1}_l(j)$, and $c^{(l)}$, for all $l \in L$ and $j \in G$
6: **for** $t = 1$ to T **do**
7: Obtain earthquake scenario $ES_t = \{m_t, r_t\}$
8: where m_t and r_t are the magnitude and location of earthquake source at time t
9: Obtain $PGA_t(j)$ $\forall j \in \mathcal{V}$
10: Obtain $S^t(j)$
11: Actualize $W_t = \mathbf{1}_l(j) * c^{(l)} * F * S^t + W_t^{(l-1)}$
12: **end for**

4.3 IEEE-118 case study

In Figure 4.3 a geographical representation of the IEEE 118 Bus Test Case is presented[15]. This Test case compiles the information of the 1962 Midwestern US power system. Since its publication, this power system is been widely used as a standard test case for power flow analysis (e.g.,[32, 49, 52, 117]). The system consists of 118 buses (i.e., nodes), 186 branches (i.e., edges), 91 load sides or substations (circles) and 54 thermal unit (squares). A geographical representation of the network is generated in order to develop the seismic simulation.

The seismic vulnerability methodology summarized in algorithm 1 was used to model this problem. According to the flow data, node 69 is the swing bus (i.e., G-29), therefore all the

[15]The information was obtained from an image of the IEEE 118 Bus available in [9]

voltages are referred to this node for the DC power flow. The net-ability value for each node is obtained using equation 1.7, from the DC power flow approximation (see section 1.2). Then, $\triangle K$ is calculated for each node.

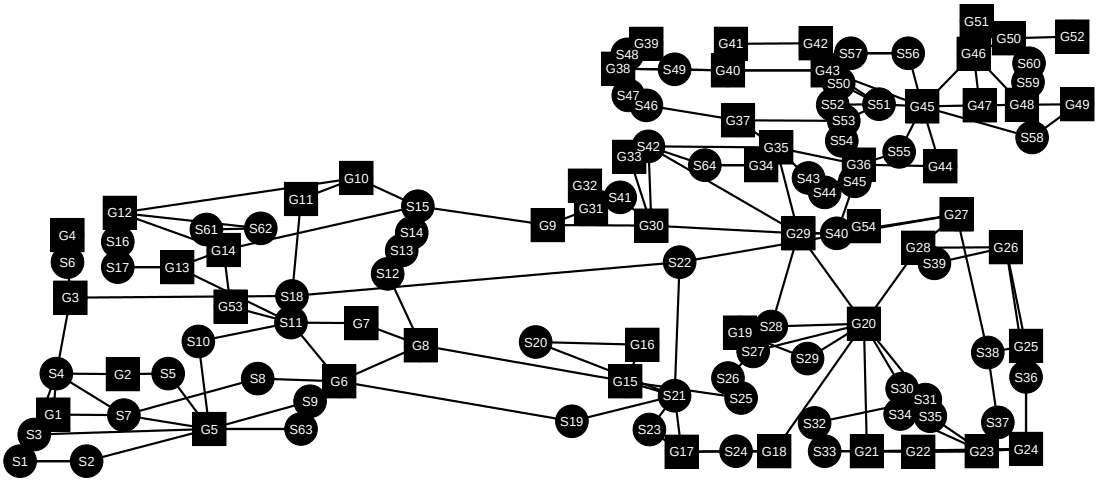

Figure 4.3: IEEE-118 Test Case network representation

The drop in net-ability ($\triangle K$), as previously mentioned, is used to represent the relative importance of each node of the network (i.e., $F(j)$). The cumulative distribution of the resulting net-ability for the IEEE-118 network is shown in Figure 4.4. A high heterogeneity is shown in the drop of net-ability.

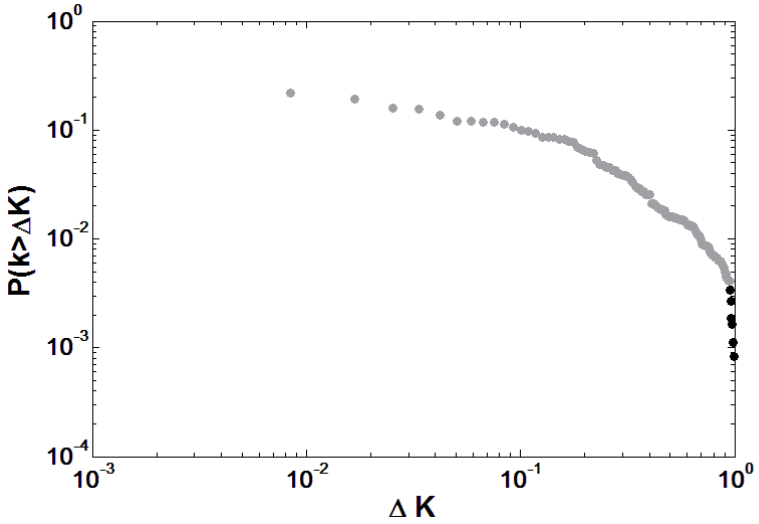

Figure 4.4: Cumulative distribution of drop in net-ability ($\triangle K$) in the IEEE-118 bus system

Most of the results lie below 0.1 (around 90 %), however few nodes can cause a high $\triangle K$.

The latter can be seen in the dark region of Figure 4.4 and it confirms the existence of critical nodes[16], whose malfunctioning can cause high consequences in the network [47]. These nodes are node # 80 (G-36), 65 (G-27), 68 (S-40), 49 (G-20), 77 (G-35) and 37 (S-21) in decreasing order.

The 2RNet software[17] is used to acquire the hierarchy of the IEEE-118 network. The clustering algorithm used is Markov clustering (MCL) [118]. This clustering technique is used as the first approach to analyse the network mainly because it is an unsupervised algorithm, which means that no a priori knowledge of graph's community structure is needed (i.e., does not require number of clusters as input). The obtained hierarchy serves as the basis to create new hierarchical structures with spectral clustering techniques. In Chapter 5 sensitivity of different clustering algorithms is undertaken.

The physical distance (d_{ij}) of the network was replaced by the electrical distance (δ_{ij}) to represent distances for the clustering process. The main reason to do so, is the approximation in the location of the buses. Since the location was gathered using extrapolation from an image, the accuracy of node location is questionable. Therefore, the hierarchical decomposition would not be a good representation of the network if distance matrix is used. On the other hand, the electrical information is not only reliable, but it also represents internal behaviour of the power system.

The resulting hierarchy is shown in Figure 4.5. It is composed of four different levels: one single unit on the top of the hierarchy; in the second level, nine clusters were found; in the third level, the clustering identified 97 clusters (i.e., d=97); and finally, in the fourth level there is a cluster per node, i.e., 118 clusters. In Figure 4.6 the fictitious network of 9 nodes (i.e., clusters) of the second level of the hierarchy is shown. The fictitious network shown in black, and the real network is in grey. Each element of the real network (118 nodes) is tagged with a letter between A to I, which corresponds to the cluster it belongs. As it can be seen, the clusters are not evident since they are dependant on equivalent impedance between buses, which is just partly related to geographical distances. Therefore, each cluster node is located where the cluster centroid is, and its size represents the number of nodes that belong to that cluster.

Then, Monte Carlo simulation is carried out (steps 8 to 12 of algorithm 1). The number of simulations was determined using the coefficient of variation (CV) of the Root Mean Square Deviation (RMSD) defined as [119]:

$$CV(RMSD) = \frac{RMSD}{\bar{x}} \tag{4.8}$$

where $\bar{x}$ is the mean of the sample, and $RMSD$ is the Root Mean Square Deviation, defined as:

$$RMSD = \sqrt{\frac{\sum_{t=1}^{N}(x_{1,t} - x_{2,t})^2}{N}} \tag{4.9}$$

[16]Notice that the figure is in logarithmic scale

[17]Developed by Risk and Reliability Research group of Universidad de los Andes, Bogota, Colombia. Available in http://www.2rsoft.tk/

to measure the average difference between two time series $x_{1,t}$ and $x_{2,t}$, for N predictions ($N = 118$ for our simulation).

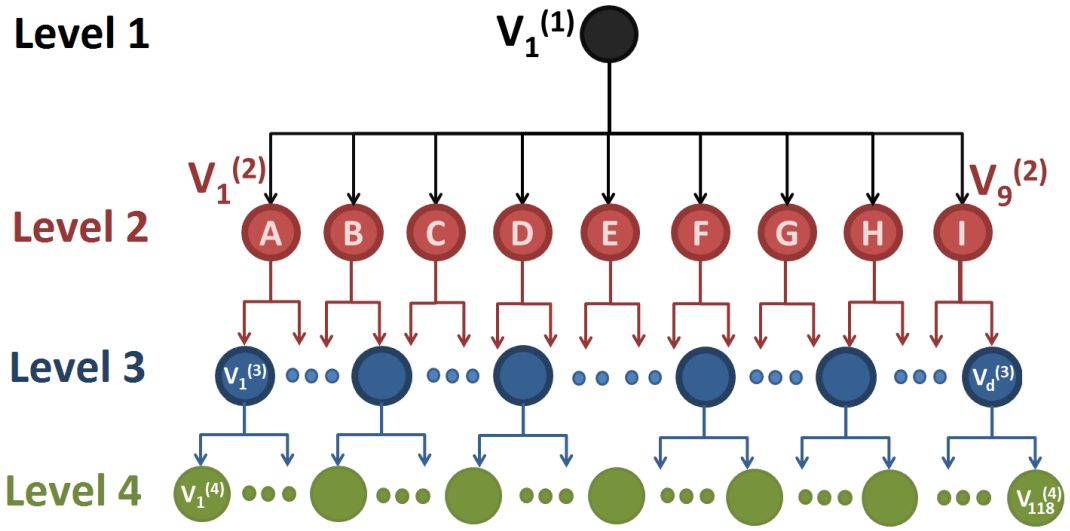

Figure 4.5: Hierarchical representation of the IEEE-118 bus system

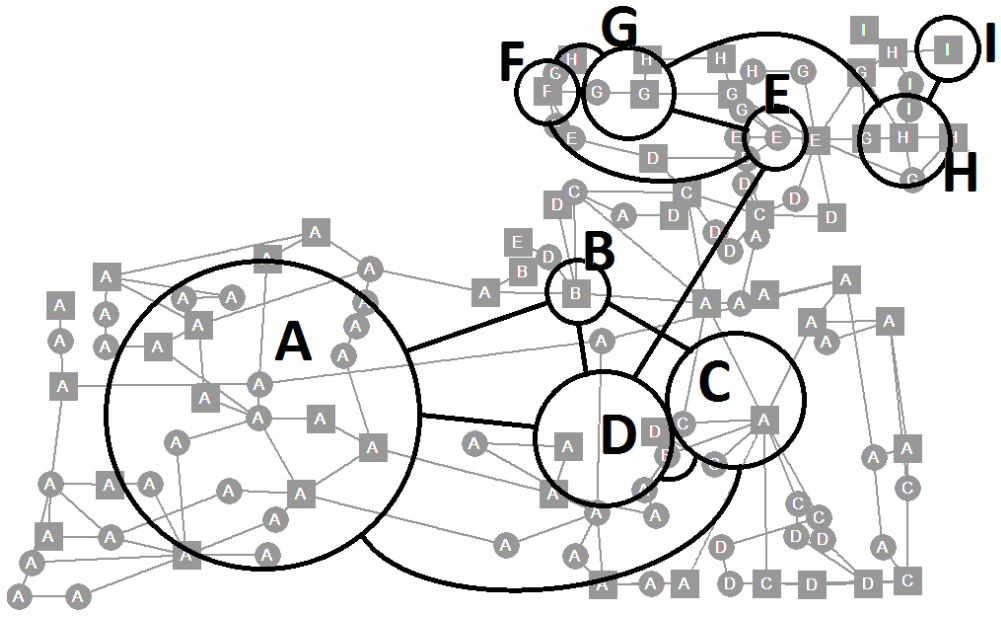

Figure 4.6: Clusters in second level of the hierarchy for IEEE-118 network

In Figure 4.7, the CV(RMSD) is shown for different numbers of Monte Carlo simulations. As it can be seen, after 500 simulations de CV(RMSD) value is very similar, therefore 500 scenarios are considered for the simulations.

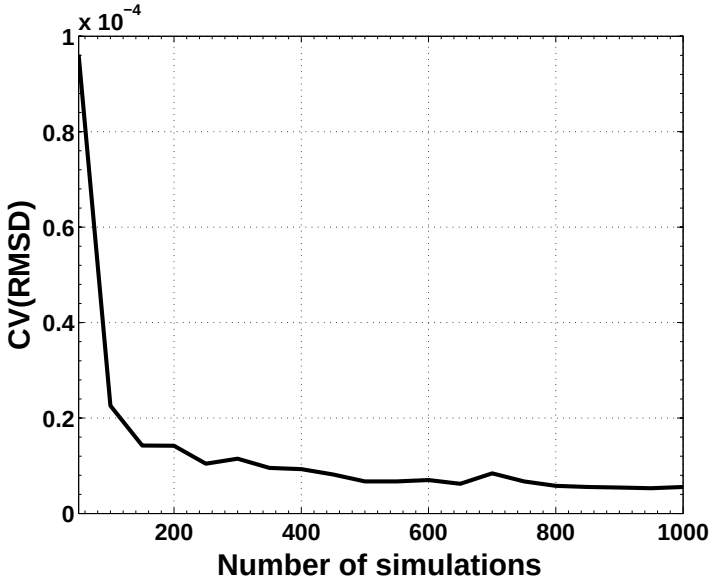

Figure 4.7: Coefficient of variation of the RMSD

Due to the lack of information regarding the seismic activity in the zone where this network was located, a simple model for the seismic hazard is developed[18]. The earthquake scenarios (ES) magnitude distribution is obtained from [101] with $M_{min} = 4.5$ and $M_{max} = 7.5$ (Figure 4.8).

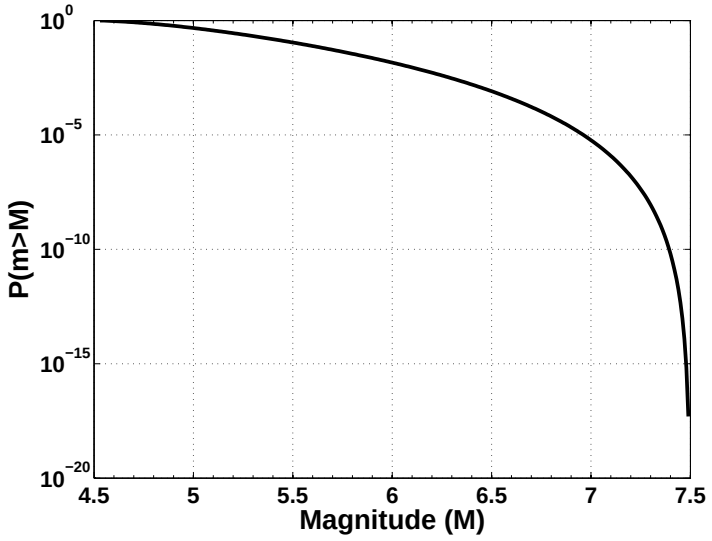

Figure 4.8: Monte Carlo simulation: a) Probability of exceedance of magnitudes.

[18]More complex seismic hazard representation can be easily incorporated into the model by replacing the attenuation equation and fragility curves

On the other hand, the epicentre is considered uniformly distributed in the area of analysis [120]. The area of simulation is circular area of 150km diameter, as shown in Figure 4.9. Current practice for seismic hazard representation assume a random distribution along a fault, however, no site information is available for this network. The distance between each node of the network and the epicentre is denoted as r in equations 4.2 and 4.10.

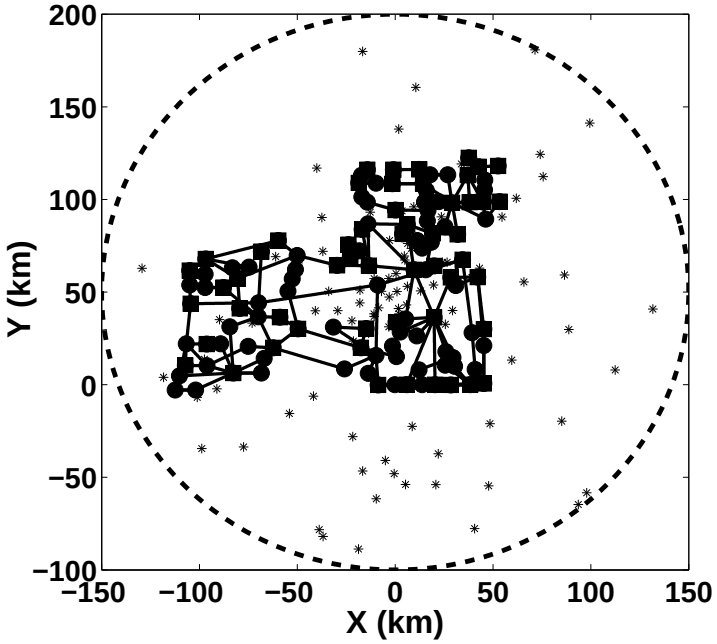

Figure 4.9: Simulation area of Monte Carlo simulation for 100 ES

Five hundred seismic scenarios were generated, where each scenario corresponds to a specific magnitude and epicentre. In each simulation, the PGA at each node is obtained using the general attenuation equation (see equation 4.1), where $b_1(r)$ is calculated as follows [101]:

$$b_1(r) = \frac{9.81 \times 0.0955}{\sqrt{r^2 + 7.3^2}} e^{-0.00587r} \tag{4.10}$$

Finally, the probability of failure and therefore, the *strength* of each element is obtained using fragility curves. As explained in section 3.1.2, fragility curves describe the probability of exceeding a specific damage level. To be consistent with the *form* measure, complete damage (CD) is selected, i.e., the substation is no longer connected to the network. For this simulation, the parameters of the fragility curves are obtain from [56], assuming unanchored substations and power plants since the data is for a network of 1962 (see Table 5.1).

In Tables B.1 to B.3 of Appendix B, the rankings obtained for different vulnerability measures are shown, as well as the respective vulnerability values for the IEEE-118 network. In the next section, these results are used for a comparison study. For now, only the hierarchical seismic vulnerability measure (represented by W) is analysed. For a better understanding, the vulnerability of each node is shown in Figure 4.10. From the resulting vulnerability measure it

can be concluded that 90% of the nodes have a vulnerability measure less than 3% of the maximum vulnerability. This result indicates that critical elements are present in the power system. Moreover, identification of such elements (i.e., most vulnerable) can be used for prioritization of retrofitting in a decision-making process (see section 4.4.1).

It is important to note that the vulnerability measure is an aggregation of *form* and *strength* and the value itself has no particular meaning unless it is analysed relative to other nodes of the same network. In Figure 4.10, the vulnerability measure for each node is shown. The nodes with black lines, represent the centroids of clusters in the second level of the hierarchy, where the letter above them corresponds to their cluster.

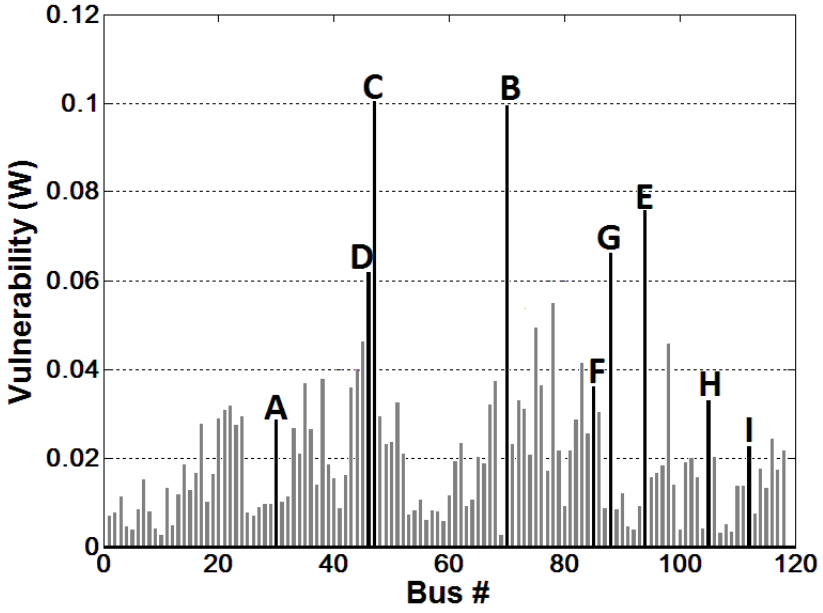

Figure 4.10: Hierarchical vulnerability measure for the IEEE-118 bus system

For this case study, it can be seen that different levels of vulnerability measure are presented. The majority of the buses have a value below 0.02 (∼58%), so this would belong to the less vulnerable nodes. Then, there is a second level of nodes with vulnerability within 0.02 and 0.04 range (∼ 33%). Even fewer nodes belong to the next level of higher vulnerability, with vulnerability measure above 0.04 and below 0.08 (∼ 7.5%); and finally, only two nodes would be the most vulnerable nodes. If nodes are grouped according to this, a hierarchy is reflected in the vulnerability measure. Therefore, this vulnerability measure not only identifies critical components, but it can also be used to developed a complete hierarchy of vulnerable elements. Moreover, by comparing the centroids, it can be seen that this hierarchy is different than the one obtained by clustering, which shows the effect of *strength* and *form*.

The resulting ranking of the vulnerability measure was compared in [121] with traditional

seismic vulnerability methodologies. The compared models in increasing order of complexity are: 1) pure connectivity method, 2) hierarchical-based vulnerability (proposed in this thesis), 3) power flow analysis based (see [71]), 4) power flow analysis with internal components (see [122]), and 5) power flow analysis with internal components and short-circuit propagation (see [122]). The spearman rank correlation factors reported of the hierarchical method compared to flow-based methods are: 0.686 with method 3; 0.647 with method 4; and 0.558 with method 5. As it can be seen, the hierarchical-based methodology presents a good ranking correlation factor with respect to flow-based methods. This results indicates that the hierarchical-based seismic vulnerability approach presents results close enough for decision making process, with respect to a full analysis (i.e., flow-based methods). However, the difference between them suggests that flow-based methods are necessary for more detail performance analysis such loss estimation and cascading analysis (see [121] for details).

4.4 Comparative study

In power systems, the results from a vulnerability assessment can be used to provide insight about the system performance and subsequently used for retrofit selection decision-making [23]. The vulnerability of an element can be measured in terms of the degree of sensitivity to specific threats [31]. Although there is not a unique vulnerability index measure, the suitability of different methods for a specific application can be compared indirectly by establishing a relative ranking (e.g., [29, 38, 47, 52]). In this section, the prioritization strategy for resource allocation is used in order to compare different vulnerability measures.

In electrical power networks, seismic retrofit can be formulated as an optimization problem. The objective can be defined as minimization of the expected losses (e.g., loss of load (LOL)) due to seismic hazard. Therefore, this is influenced by physical response of the system, such as probability of failure, maximum ground acceleration on site, and configuration of the network. Assuming a cost that is proportional to the number of retrofitted structures, the resource allocation problem can be defined as:

$$\begin{aligned} \text{minimize} \quad & E[LOL] \\ \text{subject to} \quad & N_{retrofit} \leq k \\ & R \leq L_R \end{aligned} \tag{4.11}$$

where $N_{retrofit}$ is the number of elements retrofitted, used as surrogate measure of cost; k is a pre-defined budget; and R corresponds to the resiliency of the system, which can be constrained by reliability standards L_R (e.g., [123]). Additional constraints and objectives can be included in the optimization problem depending on the decision-maker, available information, and context [71, 75, 124–127].

In this problem, a specific budget (k) is given and therefore, the decision is to identify the k elements of the network that will lead to the minimum LOL. In other words, a prioritization strategy is needed in order to find a solution. This strategy thus should consider the seismic conditions of the location, the vulnerability of the network and the electrical behaviour.

4.4.1 Prioritization for resource allocation

The process of prioritization for resource allocation is described in Figure 4.11. It consists of two main sections: the first part of the process consists of the prioritization and resource allocation and the second part consists of the evaluation process. The prioritization is performed for different budgets (i.e., number of elements, k) as follows:

1. Select the strategy, i.e., vulnerability measure.
2. Prioritize the elements according to the vulnerability measure[19] (from high to low).
3. Retrofit the first k elements according to their priority.

Several seismic retrofitting strategies have been proposed (e.g., [71], [15], [59], [128], and [129]). In this thesis, however, the retrofitting strategy is related to the prioritization of elements to retrofit. This requires identification of most vulnerable elements that improve the network performance (i.e., reduce the LOL) if retrofitted for a given seismic scenario.

Once the elements have been retrofitted, the evaluation part takes place. A Monte Carlo simulation is performed in order to evaluate the effectiveness of the vulnerability measure to identify the most critical elements. The retrofitted elements are differentiated from the unretrofitted through their fragility curves. For substations, the fragility curves reported in [112], with existing transformers and retrofitted transformers are used. On the other hand, for generation facilities, the fragility curves for complete damage reported in HAZUS [56] for anchored and unanchored are used to distinguish between them.

The Monte Carlo simulation implemented here is similar to the one described in steps 6 to 12 of Algorithm 1 (see j loop in Figure 4.11). First, a random seismic hazard is obtained and the PGA on each node is calculated. Then, the probability of failure is obtained from the fragility curve which varies depending if a node is retrofitted or not. Subsequently, the probability of failure of each node is compared with a limit state condition, e.g., a collapse threshold (γ), to know if the node is out or not. This collapse threshold is assumed to be a uniformly distributed random variable. If the final probability of failure of node i exceeds γ, the node is disconnected. As a consequence, the disconnected network is the representation of the failure caused by the seismic hazard. Finally, the LOL is calculated for the resulting network. Furthermore, it is obtained for each of the prioritization strategies under the same set of seismic scenarios.

In order to compare the strategies, different budgets are analysed, which determine how many elements can be retrofitted. At the end, the most effective strategy is determined as a multi-objective optimization, according to the resulting Pareto front comparing the number of elements retrofitted and its corresponding LOL. The Pareto front is the image of the efficient set (i.e., set of solutions in which one objective function cannot be improved without worsening the others)[130]. Therefore, identifying this frontier for each strategy will give a measure of its efficiency in the resource allocation process. In this chapter, the cost of retrofit is assumed to be proportional to the number of structures and equal for substations and generation facilities.

[19] This vulnerability measure can either only account for criticality of nodes or include as well the physical seismic damage (as in the proposed approach)

4.4.2 Vulnerability measures

As previously explained, the first step of the retrofitting prioritization strategy is the selection of the vulnerability measure (i.e., *Retrofitting allocation* in Figure 4.11). Some of the most common topological measures used for identification of critical nodes (i.e., vulnerable nodes) in power systems are: node degree [37, 39, 51, 52], and node/link betweenness [27, 29, 52]. Additionally, few topological measures have been proposed including power flow [29]. Net-ability is one of them, however it is already included in our approach. Another approach in this line is *node traffic* proposed in [52]; thus it is used for comparison.

In summary, the following three measures have been selected to compare with our hierarchical method:

- **Node degree (D)**:The degree presents an appropriate metric to compare with, since it is a representation of the connectivity of the network. Node degree is calculated for each bus of the IEEE-118 network.
- **Node betweenness (B)**: This metric evaluates the amount of flow that passes through each node. Therefore, a node with high betweenness centrality will cause high consequences in the network flow in case of removal. Node betweenness is calculated as well for each bus.
- **Node traffic (T)**: This metric is introduced in [52] to measure the traffic of each bus from a pure electrical perspective. The traffic (T) is calculated as follows[20]

$$T_i = |P_i| + \sum_{j=1}^{n} |(\theta_i - \theta_j)/x_{ij}| \tag{4.12}$$

  where θ_i is the voltage angle in node i, θ_j is the voltage angle in node j, the summation represents all the flows into and out of the bus through transmission lines. $|P_i|$ is the absolute value of net power injection into node i by generators and load, and is calculated as [52]:

$$P_i = \sum_{j=1}^{n} (\theta_i - \theta_j)/x_{ij} \tag{4.13}$$

[20]This measure is similar to a node-loading measure. However, it can only be used to identify critical nodes (i.e., nodes with maximum traffic) since it is not exactly measuring load (i.e., power) but an absolute value of it.

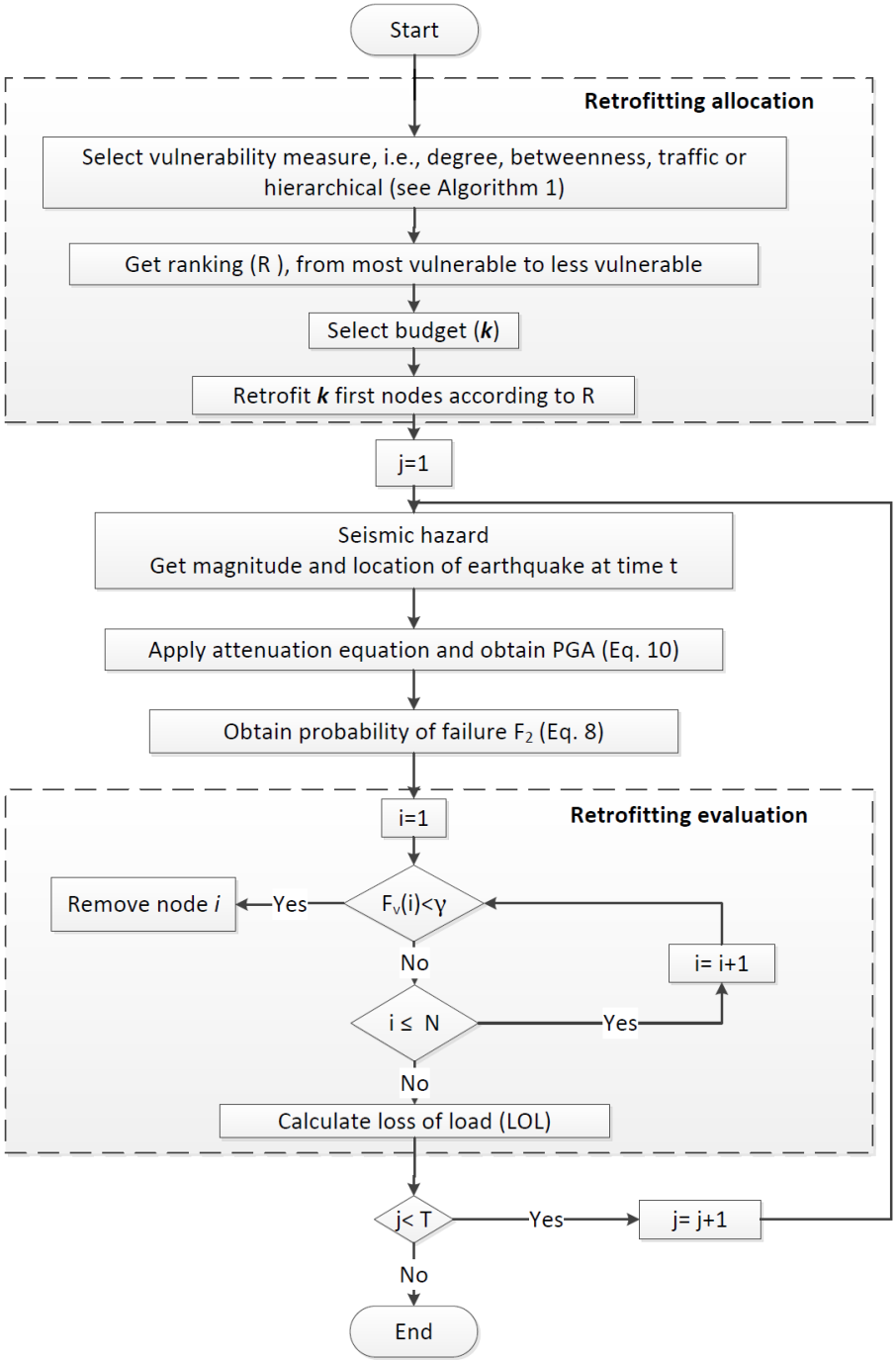

Figure 4.11: Retrofit prioritization using vulnerability

4.4.3 Results and discussion

The vulnerability values for the four measures (i.e., **D**, **B**, **T** and **W**), with their respective rankings are shown in Tables B.1 to B.3 of Appendix B. It can be observed that the scale and order of magnitude differ between measures which makes it difficult to compare. For this reason, the results can also be analysed using the relative importance of each node, i.e., the ranking position. For these measures, the methodology for retrofitting prioritization in Figure 4.11 is applied. As output, the LOL of the retrofitted network is obtained for several seismic scenarios ($T = 500$ for this simulation). Where the retrofitting process prioritize the critical nodes identified by the vulnerability measure. Thus, the distribution of the LOL gives a measure of the effectiveness of the vulnerability method to properly identify critical elements of a network in a seismic context.

In Figures 4.12, 4.13 and 4.14 the cumulative distribution of the LOL is shown, for retrofitting of 10%, 50% and 90% of the nodes, respectively. Some points of each figure are summarized in Table 4.1 to facilitate the comparison. In Figure 4.12 it can be seen that the hierarchical approach behaves better than the other measures, and identifies the most critical elements. It can also be seen, that for the degree and maximum traffic measures the elements retrofitted (i.e., 10% most critical nodes) are irrelevant to the behaviour of the network, because the LOL is equivalent to unretrofitted network (see Table 4.1).

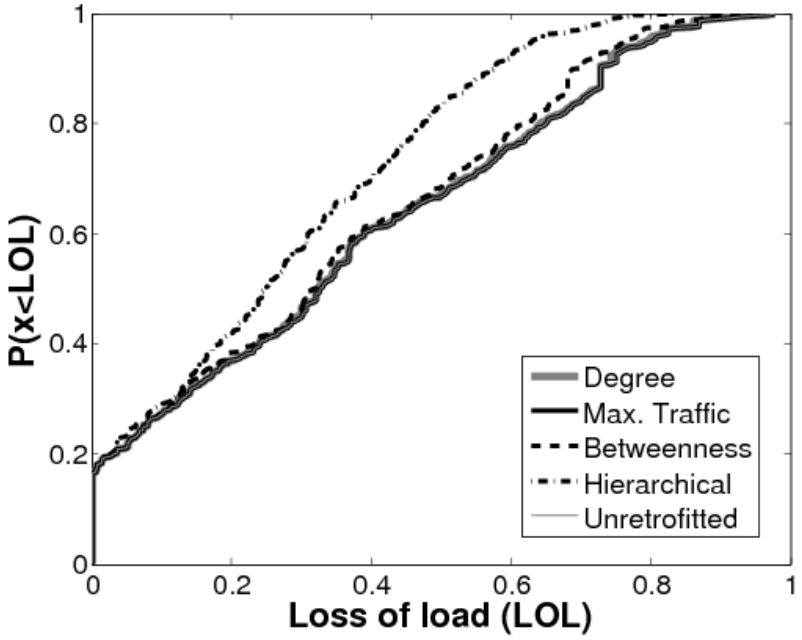

Figure 4.12: Comparison of cumulative distribution of LOL for 10% of nodes retrofitted

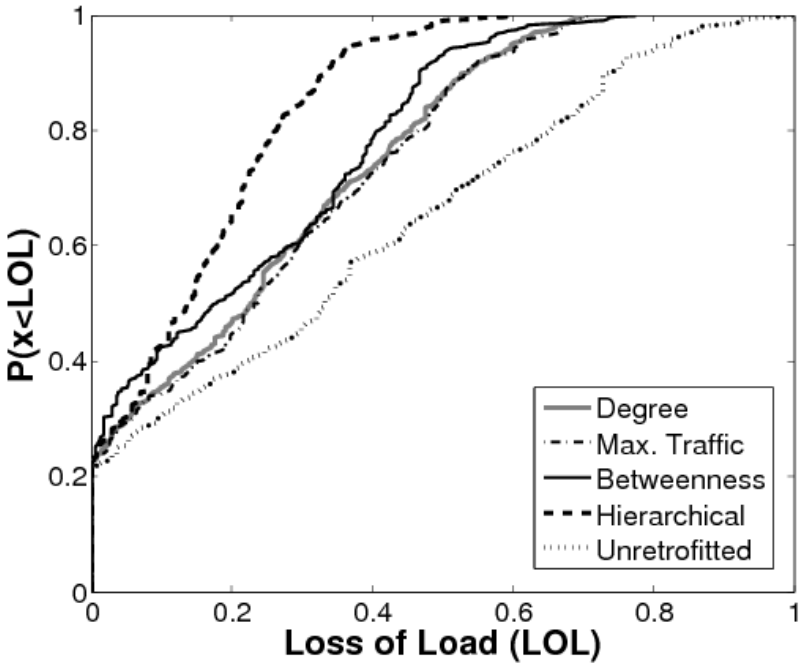

Figure 4.13: Comparison of cumulative distribution of LOL for 50% of nodes retrofitted

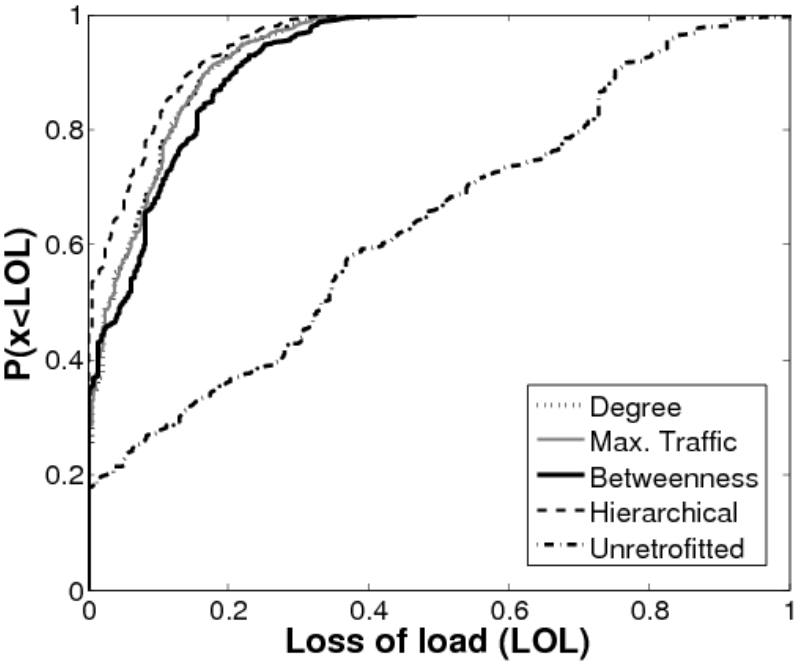

Figure 4.14: Comparison of cumulative distribution of LOL for 90% of nodes retrofitted

In Figure 4.13, the major difference between measures can be appreciated. Once again, the

Table 4.1: Comparison of retrofitting prioritization for different vulnerability measures

k	**LOL**	**Cumulative distribution of vulnerability measure**				
		Degree	Max. Traffic	Betweenness	Hierarchical	Unretrofitted
10%	0.2	0.37	0.37	0.38	0.42	0.37
	0.4	0.6	0.6	0.61	0.7	0.6
	0.6	0.76	0.76	0.8	0.93	0.76
	0.8	0.95	0.95	0.97	0.98	0.95
50%	0.2	0.46	0.44	0.5	0.64	0.37
	0.4	0.73	0.73	0.8	0.95	0.6
	0.6	0.95	0.93	0.97	0.99	0.76
	0.8	1	1	1	1	0.95
90%	0.2	0.93	0.93	0.89	0.94	0.37
	0.4	0.99	0.99	0.99	0.99	0.6
	0.6	1	1	1	1	0.76
	0.8	1	1	1	1	0.95

hierarchical approach presents the less LOL compared to the rest of the measures (see Table 4.1). Additionally, even though the LOL is improved with the other measures compared to unretrofitted network, the difference is not significant considering that 50% of the nodes have been retrofitted. This means that the other measures fail to capture critical elements for seismic hazard.

For an optimization process it is important to measure the trade-off between cost and benefit. For this particular resource allocation process, the cost is related to the number of elements retrofitted and it is constrained by the total budget. However, it is useful to know the response of the prioritization strategy for different budgets, so the efficiency of the solution can be measured.

In Figure 4.15 the Pareto front is presented for all the prioritization strategies. Since different seismic scenarios are simulated, the Pareto front is obtained when the cumulative probability is $\sim 90\%$. It can be seen, that the hierarchical approach presents the best relation for minimization of the two objectives.

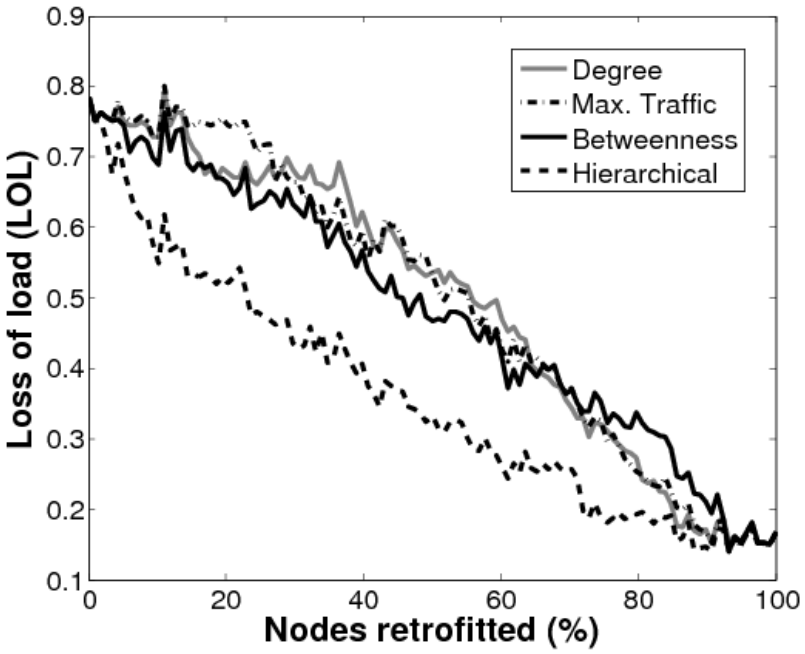

Figure 4.15: Comparison of multi-objective minimization results for prioritization strategies

Chapter 5

Sensitivity Analysis

In section 4.2, the methodology for obtaining seismic vulnerability of power networks was introduced. The hierarchical approach, combines the electrical properties and seismic hazard with the hierarchical decomposition of the system to highlight intrinsic properties of it. However, the seismic response of the system is based in the probability of failure of each element, i.e., the fragility curves selected. Therefore, a sensitivity analysis of the vulnerability measure to variation of the fragility curves is necessary to characterized the methodology.

On the other hand, the system thinking approach depends on the hierarchical decomposition of networks, which highly relies on the clustering algorithm selected. Therefore, a study on the effect of varying the hierarchy is paramount. In section 5.1, the sensitivity analysis for fragility curves is carried on for different models and type of substations. Similarly, in section 5.2, sensitivity analysis of vulnerability is presented by varying the clustering algorithms used for the hierarchical decomposition.

5.1 Sensitivity of vulnerability to fragility curves

In this section, an analysis of the vulnerability measure is developed, comparing fragility curves from different regions, and different approaches. Four approaches were selected in order to compare their impact on vulnerability measure for different type of substations structure (see Table 5.1). In Table 5.1 the parameters (mean and beta) of each of the approaches are shown. For this study, a complete damage (CD) state is considered (i.e., $P(ds > CD|PGA)$.

Among the approaches studied only HAZUS analyses generation facilities, therefore, these values are also used for generation facilities in the non-HAZUS simulations. Specifically, for Rasulo et al. [74], Duenas-Osorio et al. [65] and Hwang and Huo [112] the parameters for small generation facilities are as defined for unanchored substations in [56] (median=0.58g and beta=0.55). Similarly, the parameters for medium/high generation plants are: median=0.79g and beta=0.5. Only for HAZUS-anchored simulation, the values for generation facilities are changed as: small (median=0.78g, beta=0.5), medium/high (median=0.92g, beta=0.55).

In Figures 5.1 to 5.3, the fragility curves for different size substations are shown. The substation model from Rasulo et al. [74] is included in all of them to show the difference between a general (i.e., any size) and a specific model (i.e., specific size). Furthermore, in Figure 5.3, all references from Table 5.1 are included, to see that the seismic response of the component changes even though all of them are modelling substations, due to the specific characteristics included in each reference.

Table 5.1: Fragility curves for different substations

Ref.	Component	Median (g)	Beta
Rasulo et al. [74]	General Substation model	0.31	0.26
Dueñas et al. [65]	Low-Voltage Substation	0.45	0.44
	Medium-Voltage Substation	0.35	0.42
	High-Voltage Substation	0.2	0.35
Hwang et al. [112]	Substation with existing transformers	0.17	0.32
	Substation with retrofitted transformers	0.67	0.29
HAZUS [56]	Low-Voltage Substation (unanchored)	0.74	0.4
	Low-Voltage Substation (anchored)	0.9	0.45
	Medium-Voltage Substation (unanchored)	0.5	0.4
	Medium-Voltage Substation (anchored)	0.7	0.4
	High-Voltage Substation (unanchored)	0.38	0.35
	High-Voltage Substation (anchored)	0.47	0.4

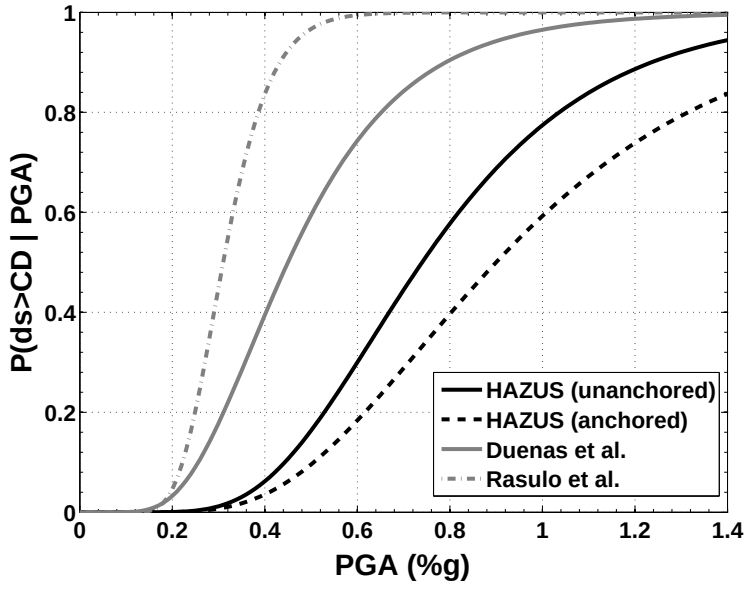

Figure 5.1: Fragility curves for complete damage of low-voltage substations

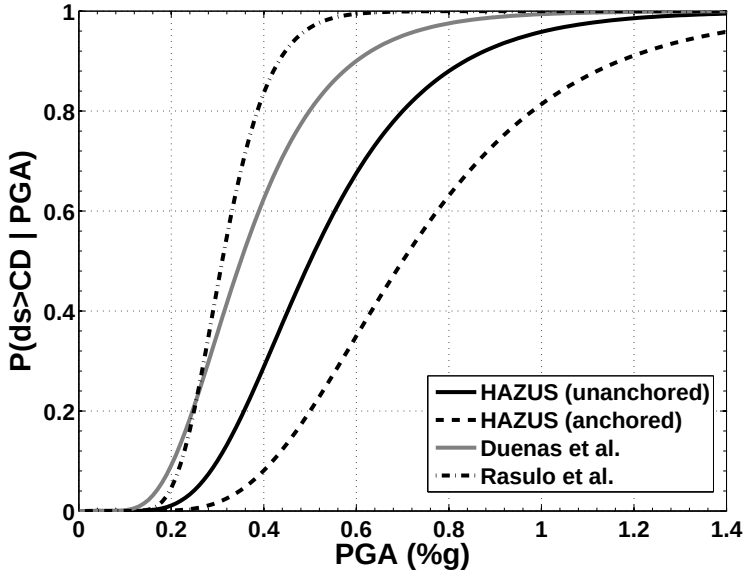

Figure 5.2: Fragility curves for complete damage of medium-voltage substations

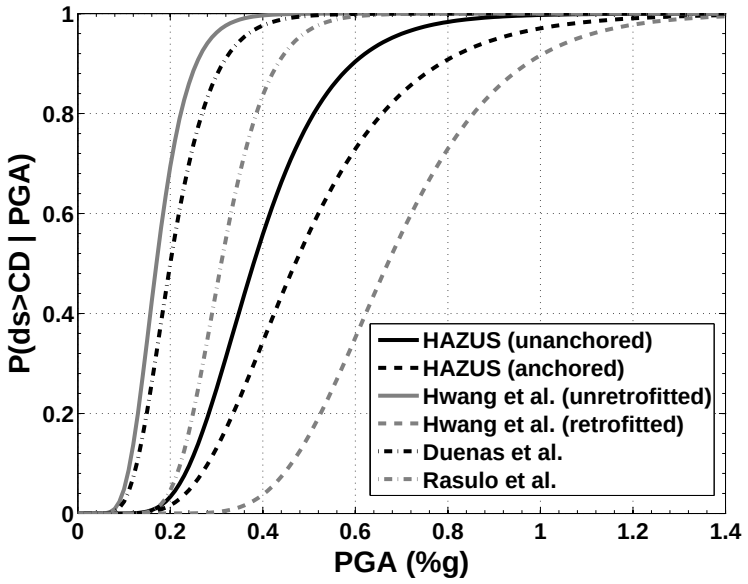

Figure 5.3: Fragility curves for complete damage of high-voltage substations

Additionally, for simulation of Rasulo et al. [74], only one fragility curve is given, consequently all substations are simulated as equal. Likewise, two type of substations are presented by Hwang and Huo [112]: with and without transformer retrofitting. These cases are simulated separately and all-size substations are given a single fragility curve. Finally, varying the values for sub-

stations, the vulnerability measure is obtained using the methodology proposed (see Algorithm 1).

The resulting seismic vulnerability measures are shown in Figure 5.4. First, comparing the final distribution of the vulnerability, it can be seen that the most vulnerable system is given by the substations with existing transformers (i.e., non-retrofitted). While on the other hand, as expected, the least vulnerable system is the system with retrofitted transformers. These results highlight the importance of the transformers in a substation and its vulnerability to failure [11].

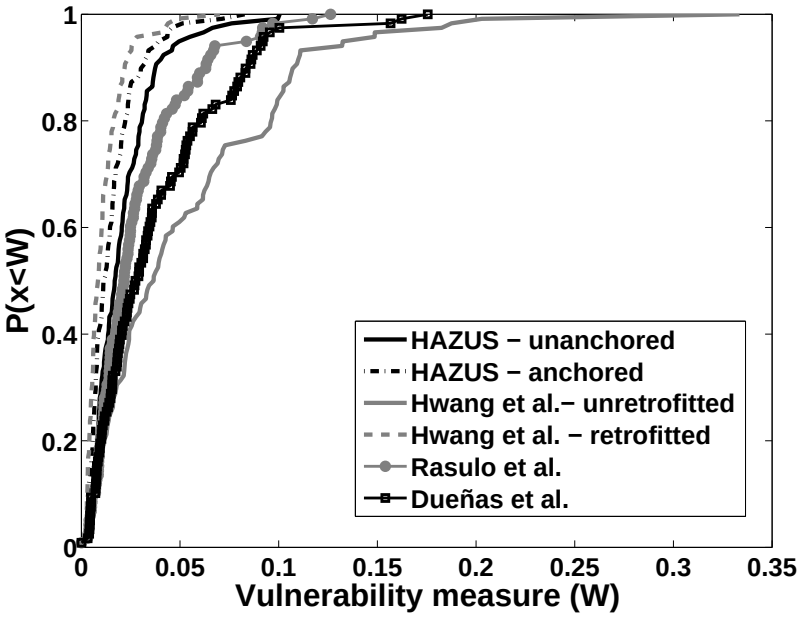

Figure 5.4: Seismic vulnerability for different substation models of complete damage

Now, comparing the models from different regions, the data shows that the Italian substation model presents a response somewhere in the middle between findings of HAZUS and Dueñas et al. (2007). Even though the last two are based in data collected in the U.S., in [56] the approach is numerical analysis, while in [65] the approach is empirical. In terms of regional differences, no reliable conclusion can be made. However, it can be concluded that the methodology selected for modelling the fragility of the substation, affect significantly the final vulnerability value. Furthermore, the numerical analysis may tend to underestimate the fragility of the substation.

Finally, the effect on the final vulnerability of the anchored vs. unanchored substations is not very relevant. This may be due to underestimating the fragility of unanchored substations or it can reflect that internal properties (i.e., system's *form*) of the system have a higher influence over the final vulnerability than the difference in anchorage of substation.

5.2 Sensitivity of vulnerability to clustering algorithms

Since the creation of the world wide web and access to vast amount of data, the research community has proposed several algorithms for solving the partitioning problem. A detailed description of different types of clustering algorithms is beyond the scope of this work. However, different surveys on clustering algorithms have been published e.g., in Jain et al. [91], the topic is addressed from a pattern recognition perspective; in Berkhin [131] the survey is developed for data mining applications; while in Xu and Wunsch [89], three perspectives of the partitioning problem are presented: statistical, computer science, and machine learning.

In this thesis, we focus our attention on spectral clustering. The main idea of these techniques is to model the clustering problem as a graph partition problem [132], which is suitable with the nature of power systems. In the following sub-section, the most known spectral clustering algorithms are explained. Subsequently, in section 5.2.2, the hierarchical decomposition using each algorithm is shown. Finally, in section 5.2.3, a comparative study of seismic vulnerability is carried on varying the hierarchy.

5.2.1 Spectral clustering

The basic idea of spectral clustering is to model the data as a graph. Given a set of data points I, a graph G is defined such that each data point is a node of the graph, and is connected to others through weighted edges. This weight depends on a similarity measure (S) between the two data points, i.e., feature distance between points ($S_{ij} = S_{ji} \geq 0$). Therefore, the clustering algorithm becomes a graph partitioning problem.

For this graph certain quantities are defined so they will be useful to normalize the similarity matrix. A *degree* vector is defined as [133]: $d_i = \sum_{j \in I} S_{ij}$, whose matrix representation (D, where $D_{ii} = d_i$ and $D_{ij} = 0$ if $i \neq j$). Likewise, the *volume* of a set $A \subset I$ is defined as $VolA = \sum_{i \in A} d_i$. Finally, the *edge cut* between two sets A and B is defined as [98]:

$$Cut(A, B) = \sum_{u \in A, v \in B} S(u, v) \tag{5.1}$$

Graph partitioning seeks to find a disjoint set of vertices that optimizes certain similarity measure. Usually, minimal spanning trees or limited neighbour set are used as efficient methodologies for graph partitioning. However, these methodologies use local properties of the graph which fail to capture the global properties of the data [98]. In the context of image segmentation, new criterion have been proposed that guarantee good partitions [92, 94, 133, 134].

According to Verma and Meila [132] the main steps of a spectral clustering algorithms, for a given similarity matrix are:

1. Preprocessing: normalization of similarity matrix.
2. Spectral Mapping: calculation of eigenvalues and some eigenvectors of normalized similarity matrix. A mapping of the data points is performed, such that each point's properties (i.e.,

dimensions) are the corresponding entries of the selected eigenvectors.

3. Grouping: simple clustering routine is performed over the new representation of the data.

In Figure 5.5, a flow diagram representing four of the most common algorithms is shown. The first one is called SM by Shi and Malik [98]. With application for image segmentation, they proposed a new 'normalized' cut criterion for the graph partitioning problem. Furthermore, they prove that optimizing this criterion leads to a partition that maximizes similarity within clusters and minimizes similarity between them. This normalized cut is defined as follows [98]:

$$NCut(A,B) = Cut(A,B)\left(\frac{1}{VolA} + \frac{1}{VolB}\right) \tag{5.2}$$

where A and B are two sets that belong to the set of data point (I); and $cut(A,B)$ and $VolA$ are the aforementioned quantities. This algorithm always finds a bi-partition of the input set. Therefore to find a partition of X clusters, it recursively applies the *normalization*, *mapping* and *grouping* steps (see flowchart in Figure 5.5) to the cluster with largest μ_2 eigenvalue until X clusters are obtained [98].

A modification of SM is proposed by Kannan et al. [94], with the algorithm called KVV. As shown in Figure 5.5, the *normalization* and *mapping* steps are the same, however the optimization criteria for *grouping* is the Cheeger conductance $\phi(C_i, C_i')$ instead of the $NCut$. If data set I is partition into to clusters C and $C' = I \backslash C$, the conductance $\phi(C, C')$ is defined as [94]:

$$\phi(C,C') = \frac{Cut(C, I\backslash C')}{\min(VolC, VolC')} \tag{5.3}$$

This algorithm also performs bipartitions in each iteration therefore, it is applied recursively until number of clusters required are obtained. However, the KVV decides the next cluster as the one with the minimum conductance. In [94], performance guarantees for this optimization criterion and recursion are included.

Another modification of SM is presented by Meila and Shi [133]. This algorithm called Multicut, uses the same normalization as in [98], but instead of finding a single partition of the data (i.e., using only u^2), it maps the data points according to the X eigenvectors $u^1, u^2, ..., u^X$ corresponding to the largest eigenvalues (see Figure 5.5). Finally, the *grouping* step is done applying K-means to the new representation of data points, given by the eigenvectors.

Finally, Ng et al. [134] proposed a methodology based in a different normalization of the similarity matrix (NJW Algorithm). In contrast to SM/KVV/Multicut, it uses the *Lapacian* of the similarity matrix to get the X largest eigenvalues with its corresponding eigenvectors. The latter, are used to find the best partition by stacking the eigenvectors in the columns of matrix U such that each data point has X dimensions. However, this representation is first normalized so that the rows in U have a unit length (i.e., $\sum_{i \in I} U_{ij} = 1$). Finally, K-means-orthogonal algorithm [132] is applied to group the points (see Figure 5.5).

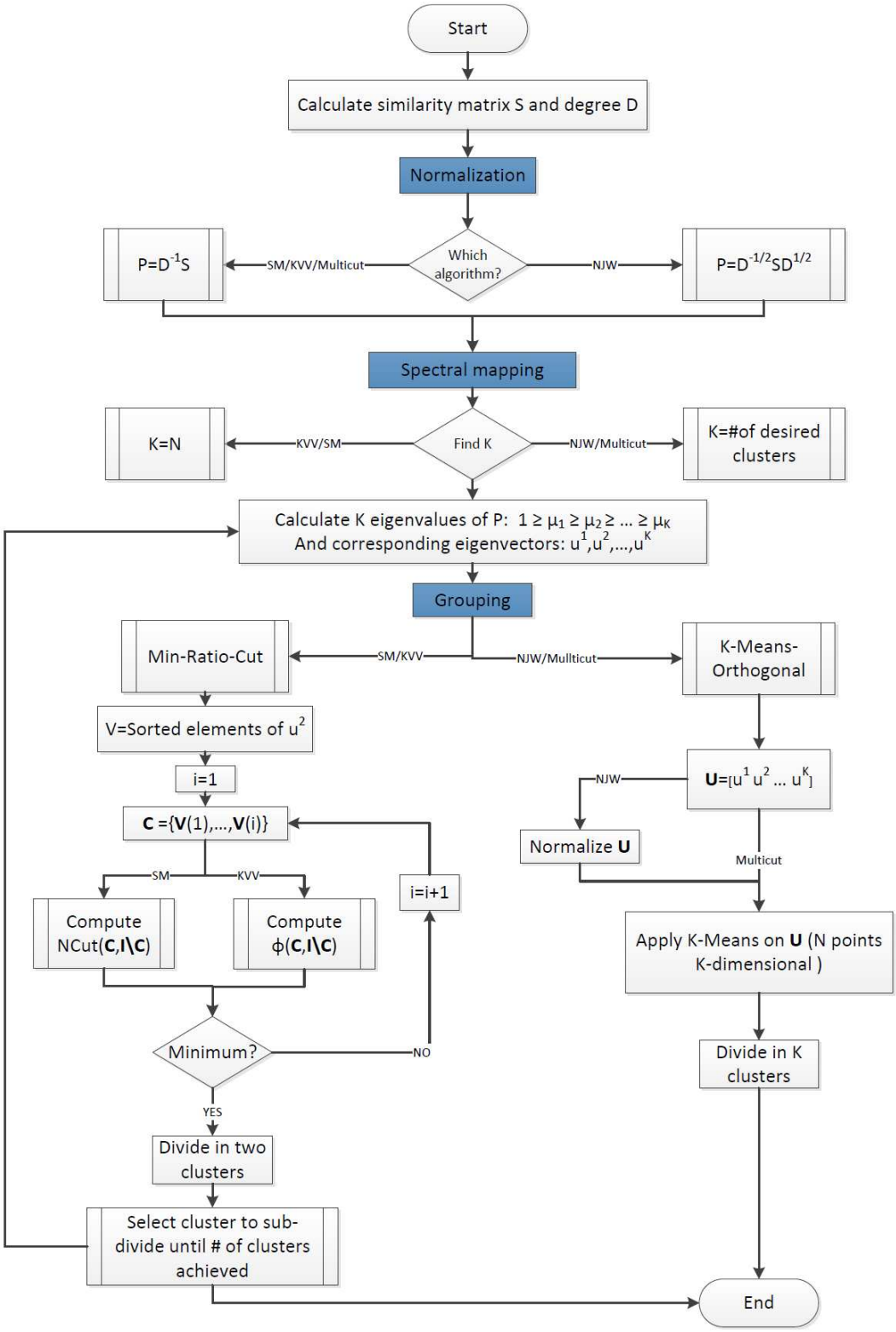

Figure 5.5: Spectral clustering algorithms

5.2.2 Hierarchical decomposition

The case study used is again the IEEE-118 Test case (see Figure 4.3). Therefore, the hierarchy obtained using unsupervised clustering (MCL) is used to initialize the spectral clustering algorithms in the second level of the hierarchy. In other words, K (see Figure 5.5) is equal to number of fictitious nodes in second level of MCL-hierarchy, i.e., nine clusters. As previously mentioned, in the first level of the hierarchy there is only one fictitious node, composed of all the nodes in the graph.

SM clustering

Using the SM algorithm, the fictitious networks shown in Figure 5.6 are found. In the second level of the hierarchy only two clusters were found, where basically one substation (S-49) is separated from the rest of the nodes. Although this is not a common partition, it is the one that minimizes the normalized cut (see equation 5.2). The reason why this node is separated basically yields in a relatively high equivalent impedance, and the fact that is only connected to two nodes, which results in a low similarity measure even with its neighbours.

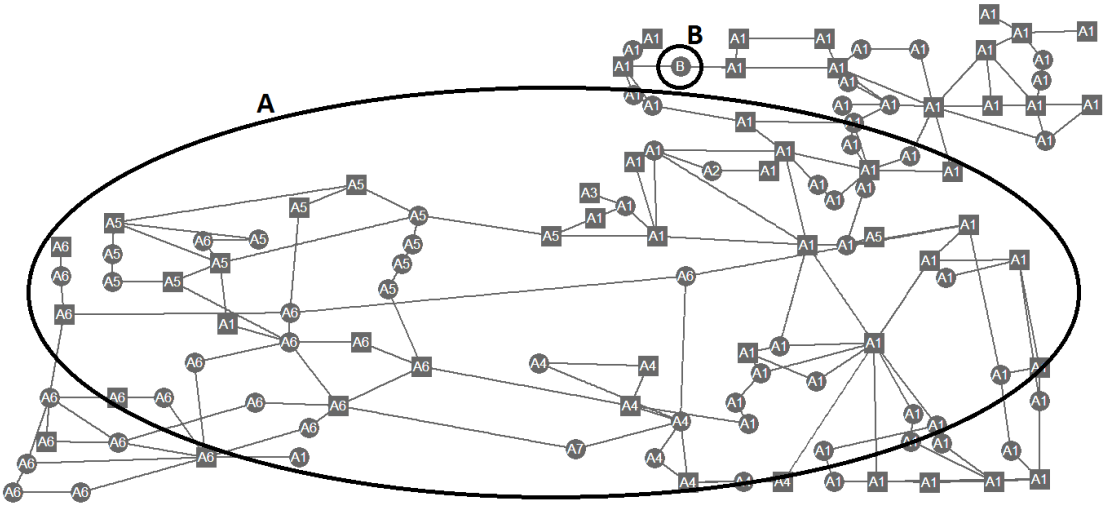

Figure 5.6: Second and third level of hierarchy using SM clustering algorithm

On the third level of the hierarchy, the biggest cluster (whose centroid is node S-40[21]) is divided into seven sub-clusters. In Figure 5.6, clusters in level 2 are identified by the letters A and B, and the numbers following this letter correspond to the clusters in the third level. Finally, in the last level, each real node is a fictitious node (cluster).

It is important to mention that even though the number of clusters k is given, there is stability criteria based on the eigenvectors, which controls whether a recursion should be make or not, therefore the number of clusters in each level may not be the k value (for details see [98]). This

[21]The centroid of a cluster is obtained as the node that has the highest similarity measure with the rest of the nodes in the cluster

is actually what happens in levels 2 and 3 for the IEEE 118 network. We want to have 9 clusters, to follow communities found with MCL, but we can only partition the network in 2 clusters for the second level (i.e. $V_1^{(2)}$ and $V_2^{(2)}$). Similarly, in the third level, we want to partition biggest cluster[22] $V_2^{(2)}$ into nine sub-communities, but only seven are possible due to the stability criteria i.e., $V_2^{(2)} = \{V_2^{(3)}, ..., V_8^{(3)}\}$).

KVV clustering

As shown in Figure 5.5, by applying small changes to SM, we can obtained the KVV algorithm. The hierarchy obtained using this algorithm is as follows: in the first level, we have one single fictitious node; in the second level, nine clusters can be obtained; in the third level 29 fictitious nodes are found, corresponding to partitions of previous nine clusters; and finally, in the fourth level 118 nodes are the fictitious nodes. Similarly, in Figure 5.7 the second and third level of hierarchy are shown. In this figure, the fictitious network of the second level is represented by the black nodes, where the size of the node represents number of nodes that belong to that cluster. On the other hand, the third level is represented by the number in each node of real network (grey network).

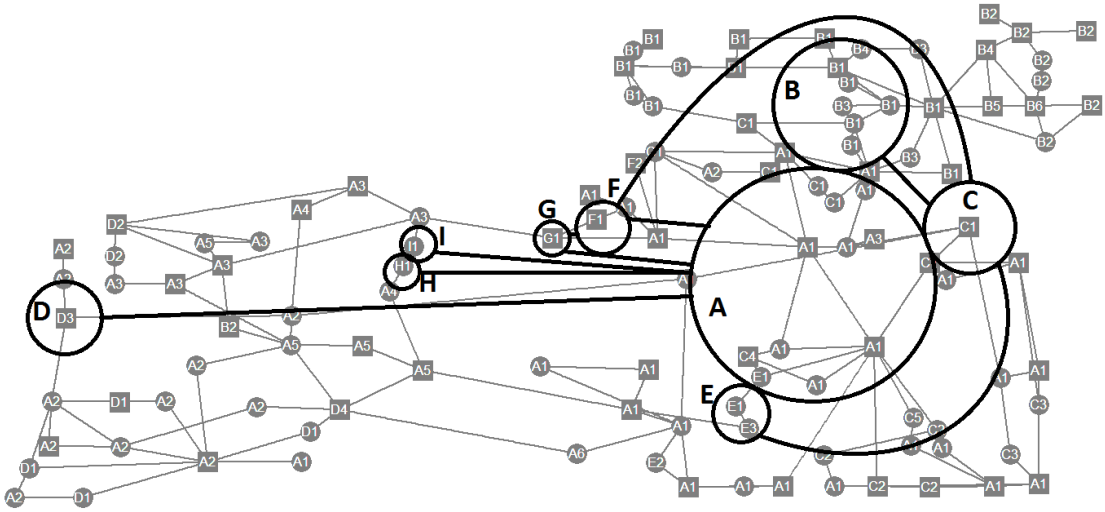

Figure 5.7: Second and third level of hierarchy using KVV clustering algorithm

NJW clustering

For the clustering algorithm presented in Ng et al. [134] (NJW), the hierarchy has 1 node in the top, 9 fictitious nodes in the second level, 50 fictitious nodes in the third level, and 118 nodes in the fourth level. In Figure 5.8, the fictitious network for second level is presented (in black), as well as the third level, represented by the numbers in the real network (in gray). The nodes in the second level are more evenly distributed, i.e., size of the node is similar. This is due to

[22]The other cluster $V_1^{(2)}$ is composed of one node (S-49) and therefore it cannot be subdivided i.e., $V_1^{(2)} = \{V_1^{(3)}\}$

the fact that the previous two algorithms find the next cluster based on a binary subdivision (recursive clustering), therefore every next cluster is usually smaller than the previous ones.

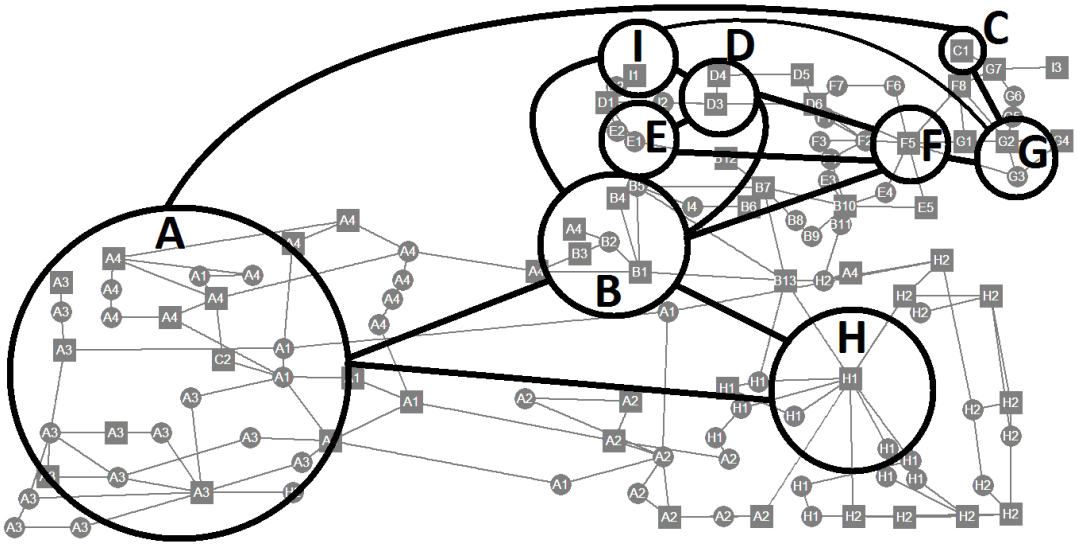

Figure 5.8: Second and third level of hierarchy using NJW clustering algorithm

In contrast, NJW uses the k eigenvectors corresponding to the k smallest eigenvalues, to partition the network. So, there is no recursion to find the k clusters of each level of the hierarchy, in other words, each level of hierarchy requires only one run of the algorithm per cluster in the upper level. However, the first cluster (cluster A in Figure 5.8) is composed of 47 real nodes, becoming the biggest cluster in the second level.

Multicut clustering

The hierarchy is obtained for the modification of SM proposed by Meila and Shi [133]. Similar to NJW, the partition is made with the eigenvectors corresponding to the k smallest eigenvalues, but using the normalization proposed in [98]. The hierarchy obtained has the same number of clusters per level as found with NJW, but with different members. In Figure 5.9 the fictitious network for second level, and partition for third level is shown.

For this hierarchy, the biggest cluster is cluster G (see Figure 5.9), with 30 real nodes on it. Nevertheless, in general the partition is even among the clusters for second and third level, as shown by the sizes of the fictitious nodes. Again, this is due to the fact that the partition is not done recursively, but using k eigenvectors.

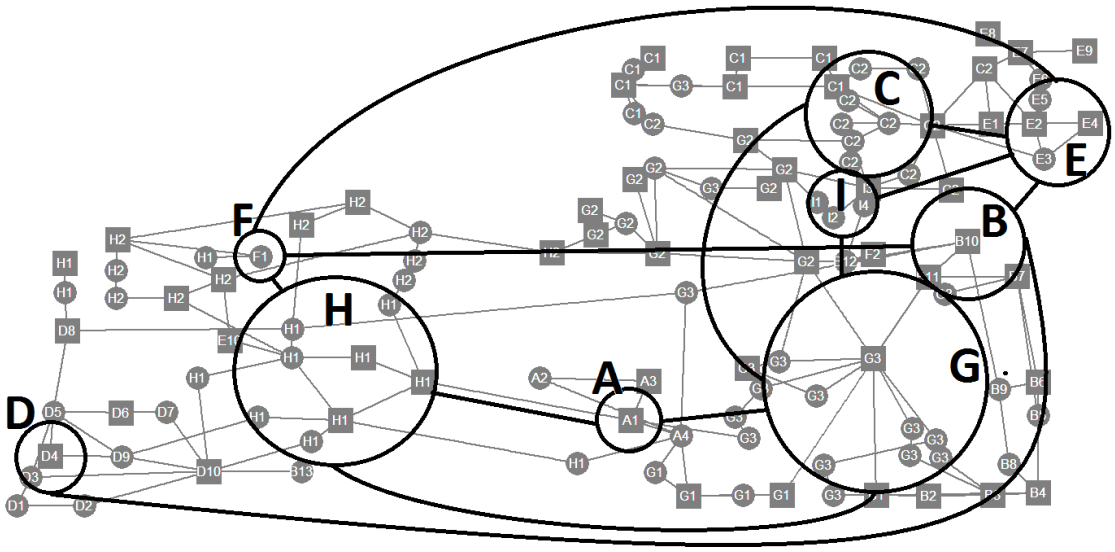

Figure 5.9: Second and third level of hierarchy using Multicut clustering algorithm

5.2.3 Comparison study

The Monte Carlo simulation is developed for 500 earthquake scenarios, considering each of the possible hierarchies. In each scenario, the vulnerability is calculated for the initial clustering algorithm (i.e., MCL), as well as for each of the hierarchies from spectral clustering. So, that we can compare same hazard and failure of the network.

The statistical mean of the vulnerability measure is shown in Figure 5.10 for each of the techniques. As shown in Figure 5.10, the hierarchical decomposition highly affect the identification of critical components, since not all the same nodes are identified as critical. However, there are patterns and critical nodes shared among the representations. First, it is clear that nodes between 68 and 98 (i.e., S-40 to S-54 and G-29 to G-44) present a tendency to have higher vulnerability compared to the majority of the nodes, and this is similar using all hierarchical representations.

Among the *critical area*, i.e., zone where most vulnerable nodes are located, there are six nodes that are identified by all or a group of the approaches as critical nodes. These nodes are: node 68 (S-40), 70 (G-30),78 (S-43), 79 (S-44),88 (S-49), and 95 (S-52)[23]. First of all, note that majority of the nodes are substations, a closer look at these substations give us the reason of such high vulnerability. The vulnerability measure is a combination of *strength*, *form* and hierarchical representation. Any combination with high value of all of them (or some), can result in a high value of vulnerability. This is the case for the substations as explain as follows.

[23]The numbers in parenthesis are the notation given in the graph representation of IEEE-118 network. See Figure 4.3 of section 4.3.

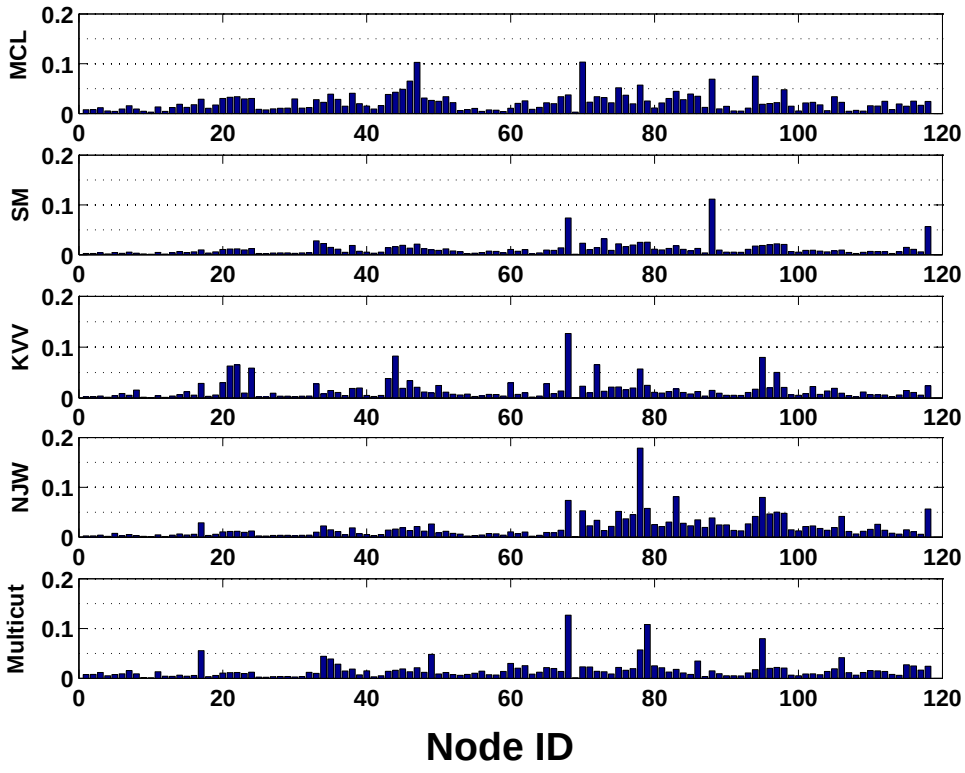

Figure 5.10: Seismic vulnerability measure for different clustering algorithms

As previously mentioned, there is no knowledge about soil type, location, or close seismic faults to the IEEE-118 power system therefore, the probability of failure provide at the end of the Monte Carlo simulation shows a similar failure measure for the same type of structure (substation or generation)[24], giving a higher weight to most vulnerable structures. Analysing the fragility curves of FEMA [56], the substations are more vulnerable to seismic hazard than the generation facilities, therefore the *strength* factor of a substation will be higher.

On the other hand, studying the *form* of these substations, show us that most of them have a $\triangle K$ that is moderate but not among the highest, which indicates that the form did not provide a high influence to the final vulnerability value. However, the clustering algorithms are based in a similarity measure and it can be seen that all of them have a very high value of similarity with the rest of the network. This implies that the equivalent impedance is small compared to the rest of the network, which can facilitate the flow of power through these nodes, becoming critical nodes.

In contrast to critical substations, the generation bus (G-30) presents a very high $\triangle K$ (2nd in the ranking), which indicates that its disconnection causes a drop in the effectiveness of flow

[24]In case of a real power system, identification of faults would change the hazard representation. In that case, distance, soil type and type of structure will influence the *strength* factor

through the network. So, even though it is not a centroid of a 1st or 2nd level fictitious node in the more than one hierarchical representation, it is a critical node mainly due to its *form* measure and this is reflected in the final value of vulnerability.

In contrast to the critical nodes identified by all, most of the nodes present different values depending on the clustering algorithm used. For this reason, we can conclude that the selection of the clustering algorithm, moreover the hierarchical representation of the system, is an important part of the process and should correctly highlight the dynamics of the system. Nevertheless, the most critical nodes are identified by all measures and they can be used for decision making.

Finally, in Figure 5.11 the distribution of the seismic vulnerability is shown, using the hierarchical representation obtained by varying the clustering algorithm. The extreme results are given by MCL and SM. The vulnerability curve given by SM, shows that the majority of the nodes have a very low vulnerability, while very few nodes have very high vulnerability. The hierarchical representation for SM algorithm is form by one node in the top, followed by two nodes in the second level and eight clusters in the third level. Since the higher weight is granted to centroids of top of the hierarchy, having few clusters in the top results in few nodes with high weight into the final vulnerability, and therefore very few nodes are identified as critical.

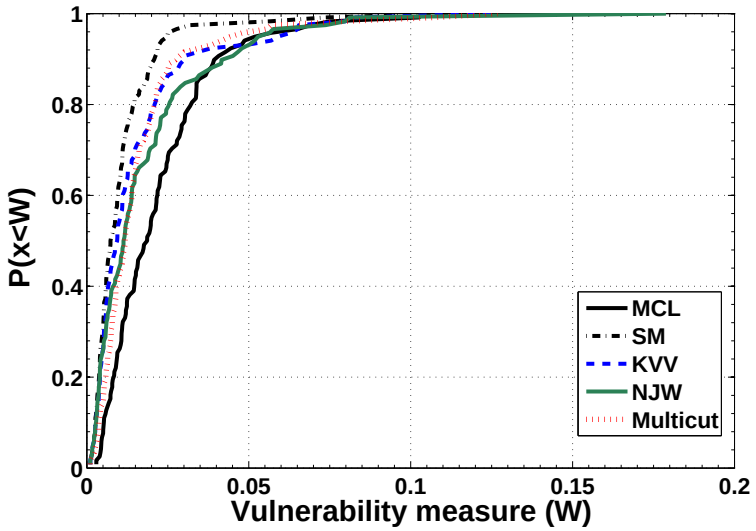

Figure 5.11: Cumulative distribution of seismic vulnerability for different clustering algorithms

In the other extreme case, the curve for MCL shows slower increment, which is also influenced by the hierarchy. Additionally to the (10) centroids in first and second level of the hierarchy, the clustering process in MCL identifies 97 clusters in the third level, which grants certain weight to the majority of the nodes. As a result, the vulnerability measure is increased for most of the nodes, just from the contribution of the hierarchical approach.

Chapter 6

Conclusions and Future Work

A novel methodology for seismic vulnerability was proposed, integrating concepts of *form* and *strength* of a power network to represent the system behaviour. A hierarchical decomposition of networks was implemented to extract the relevant information regarding the topological and electrical dynamics of power systems. Finally, a seismic information about the network is integrated in the model, resulting in representative seismic vulnerability measure that can be used for decision-making process.

The seismic vulnerability approach introduces a trade–off between the probability of failure of an specific node and the relative importance of it (*strength vs. form*). This trade–off is reflected in the results for the IEEE-118 network. Substations were found to be more likely identified as critical nodes, due to less resistance to seismic hazard. However, only substations with high importance in power flow are among the top vulnerable nodes. On the other hand, even though generation facilities are highly resistant to seismic hazard, the importance in the flow of the power network is enough to result in a high vulnerability.

Additionally, a hierarchy of critical nodes can be extracted directly from the vulnerability measure. Highlighting the hierarchical nature of the approach. Moreover, the results are consistent with previous topological analysis that identified a self-organized criticality behaviour in the power grid, i.e., few nodes are the most critical ones.

On the other hand, when comparing our approach in a decision-making process it can be seen that the hierarchical approach presents a better approximation of the seismic vulnerability. First, the cumulative distribution of LOL reveals that the hierarchical approach tends to have a less LOL independently from the number of nodes retrofitted. Moreover, this appropriate representation is generalized for all the seismic scenarios. From this comparison it is also notable that the rest of the metrics have a similar behaviour with one another. The results also show that pure topological metrics are comparable with electrical metrics in the context of seismic retrofitting prioritization for power systems. Further analysis should be done to extend this comparison to other networks.

The sensitivity results show a moderate difference in the vulnerability measure depending on the clustering algorithm, which indicates that the selection of the clustering algorithm is a key element for identification of critical nodes. However, the trade–off between *strength* and *form* is presented, identifying similar groups of critical nodes for different clustering algorithms. The results show that even though higher weights are given to cluster centroids (i.e., influence of hierarchy), the resistance of the structure to seismic damage (*strength*) and the importance of

the element over power flow dynamics (*form*) play a significant role in the vulnerability measure.

Different simplifications regarding the power flow dynamics of the power system were undertaken in this thesis. The author considers that integration of cascading analysis is among the most relevant to proceed as future work. Multiple approaches have been proposed for cascading analysis of complex systems using pure topological approach (e.g., [39, 135–137]). However only few approaches have pursued aggregation of both topological and electrical (e.g., [138, 139]) into cascading analysis of lifelines. Integration of these type of analysis into the hierarchical approach would be a more realistic approach and might enhance the vulnerability measure.

Bibliography

[1] J. Buritica, S. Tesfamariam, and M. Sánchez-Silva, "Seismic vulnerability assessment of power transmission networks using complex-systems based methodologies," in *15th World Conference on Earthquake Engineering*, no. 3418, Lisbon, Portugal, Sept 24–28 2012.

[2] B. Carreras, D. Newman, I. Dobson, and A. Poole, "Evidence for self-organized criticality in a time series of electric power system blackouts," *Circuits and Systems I: Regular Papers, IEEE Transactions on*, vol. 51, no. 9, pp. 1733–1740, 2004.

[3] J. Romero, "Lack of rain a leading cause of indian grid collapse," *IEEE Spectrum*, 2012.

[4] W. Yu and M. G. Pollitt, "Does liberalisation cause more electricity blackouts? evidence from a global study of newspaper reports," University of Cambridge, Tech. Rep. 0902, 2009, electricity Policy Research Group.

[5] F. A. Shaikh, D. Gautam, N. Pandey, and D. Singh, "International grid: New way to prevent blackouts," *International Journal of Computer Science and Informatics*, vol. 1, no. 4, pp. 2231–5292, 2012.

[6] Task-Force, "Final report on the august 14, 2003 blackout in the united states and canada: Causes and recommendations," U.S.–Canada Power System Outage Task Force, Tech. Rep., april 2004.

[7] D. E. Nye, *When The Lights Went Out. A History of Blackouts in America*. Cambridge, MA: MIT Pres, 2010.

[8] L. Wenyuan and P. Choudhury, "Probabilistic transmission planning," *Power and Energy Magazine, IEEE*, vol. 5, no. 5, pp. 46–53, 2007.

[9] *NERC*, "Reliability standards for the bulk electric systems of north america," North American Electric Reliability Corporation, Tech. Rep., 2005, princeton, NJ.

[10] A. J. Schiff, "The loma prieta, california, earthquake of october 17, 1989: Lifelines," U.S. Geological Survey, Tech. Rep. Paper 1552-A.

[11] A. J. Schiff, Ed., *Guide to Improved Earthquake Performance of Electric Power Systems*, ser. ASCE Manuals and Reports on Engineering Practice. New York: American Society of Civil Engineers (ASCE), 1999, no. 96.

[12] R. M. Chung, D. B. Ballantyne, E. Comeau, T. L. Holzer, D. Madrzykowski, A. J. Schiff, W. C. Stone, J. Wilcoski, R. D. Borcherdt, J. D. Cooper, H. S. Lew, J. Moehle, L. H. Sheng, A. W. Taylor, I. Bucker, J. Hayes, E. V. Leyendecker, T. O'Rourke, M. P. Singh,

and M. Whitney, "January 17, 1995 hyogoken-nanbu (kobe) earthquake: Performance of structures, lifelines, and fire protection systems," National Institute of Standards and Technology, Gathersburg, MD, Tech. Rep. NIST SP 901, July 1996.

[13] J. Eidinger and A. K. Tang, "Christchurch, new zealand earthquake sequence of mw 7.1 september 04, 2010; mw 6.3 february 22, 2011; mw 6.0 june 13, 2011: lifeline performance," ASCE, Monograph 40, 2012.

[14] B. Wang, D. You, X. Yin, Q. Chen, K. Wang, H. Liu, and H. Hou, "A method for assessing power system security risk," in *Power and Energy Engineering Conference (APPEEC), 2010 Asia–Pacific*, Chengdu, China, 2010, pp. 1–5, march 28–31.

[15] A. J. Schiff, *Earthquake Engineering Handbook*. CRC Press, 2003, ch. Electrical Power Systems.

[16] C. Liu and F. Feng, "Seismic security analysis and flow load control of power supply system," in *Information Acquisition, 2006 IEEE International Conference on*, Weihai, Shandong, 2006, pp. 1239–1243, aug. 20–23.

[17] W. Li, J. Zhou, K. Xie, and X. Xiong, "Power system risk assessment using a hybrid method of fuzzy set and monte carlo simulation," *Power Systems, IEEE Transactions on*, vol. 23, no. 2, pp. 336–343, 2008.

[18] F. Xiao and J. McCalley, "Power system risk assessment and control in a multiobjective framework," *Power Systems, IEEE Transactions on*, vol. 24, no. 1, pp. 78–85, 2009.

[19] E. Ciapessoni, D. Cirio, S. Massucco, A. Pitto, and F. Silvestro, "A probabilistic risk assessment approach to support the operation of large electric power systems," in *Power Systems Conference and Exposition, 2009. PSCE '09. IEEE/PES*, Seattle, Washington, 2009, pp. 1–8, march 15–18.

[20] Y. Xingbin and C. Singh, "A practical approach for integrated power system vulnerability analysis with protection failures," *Power Systems, IEEE Transactions on*, vol. 19, no. 4, pp. 1811–1820, Nov. 2004.

[21] A. Koonce, G. Apostolakis, and B. Cook, "Bulk power risk analysis: ranking infrastructure elements according to their risk significance," *Electrical Power and Energy Systems*, vol. 30, pp. 169–183, 2008.

[22] A. Pinar, J. Meza, V. Donde, and B. Lesieutre, "Optimization strategies for the vulnerability analysis of the electric power grid," *SIAM J. on Optimization*, vol. 20, pp. 1786–1810, 2010.

[23] NERC, "Security guidelines for the electricity sector: Vulnerability and risk assessment," North American Electric Reliability Corporation, Tech. Rep., 2002, june 14. [Online]. Available: http://www.nerc.com/files/Vulnerability--Assessment.pdf

[24] A. von Meier, *Electric Power Systems: A Conceptual Introduction*, E. Desurvire, Ed. John Wiley & Sons, Inc., 2006.

[25] X.-F. Wang, Y. Song, and M. Irving, *Modern Power Systems Analysis*. Spring Street, New York, NY, USA: Springer, 2008.

[26] V. Latora and M. Marchiori, "Vulnerability and protection of infrastructure networks," *Physical Review E*, vol. 71, no. 1, p. 15103, 2005.

[27] S. Arianos, E. Bompard, A. Carbone, and F. Xue, "Power grid vulnerability: A complex network approach," *Chaos: An Interdisciplinary Journal of Nonlinear Science*, vol. 19, no. 1, pp. 1–6, 2009.

[28] G. Chen, Z. Y. Dong, D. J. Hill, and G. H. Zhang, "An improved model for structural vulnerability analysis of power networks," *Physica A: Statistical Mechanics and its Applications*, vol. 388, no. 19, pp. 4259–4266, 2009.

[29] E. Bompard, D. Wu, and F. Xue, "Structural vulnerability of power systems: A topological approach," *Electric Power Systems Research*, vol. 81, no. 7, pp. 1334–1340, 2011.

[30] R. D. Christie, "Power systems test case archive," University of Washington, Tech. Rep., 1999. [Online]. Available: http://www.ee.washington.edu/research/pstca/index.html

[31] A. J. Holmgren, "Quantitative vulnerability analysis of electric power networks," Ph.D. dissertation, Royal Institute of Technology, 2006.

[32] E. Bompard, E. Pons, and D. Wu, "Extended topological metrics for the analysis of power grid vulnerability," *Systems Journal, IEEE*, vol. 6, no. 3, pp. 481–487, sept. 2012.

[33] B. Carreras, V. Lynch, I. Dobson, and D. Newman, "Dynamical and probabilistic approaches to the study of blackout vulnerability of the power transmission grid," in *System Sciences, 2004. Proceedings of the 37th Annual Hawaii International Conference on*, Jan. 2004.

[34] J. Ma, Z. Huang, P. C. Wong, T. Ferryman, and P. Northwest, "Probabilistic vulnerability assessment based on power flow and voltage distribution," in *Transmission and Distribution Conference and Exposition, 2010 IEEE PES*, Chicago, Illinois, 2010, pp. 1–8, may 7–10.

[35] A. Haidar, A. Mohamed, and F. Milano, "A computational intelligence–based suite for vulnerability assessment of electrical power systems," *Simulation Modelling Practice and Theory*, vol. 18, pp. 533–546, 2010.

[36] D. J. Watts and S. H. Strogatz, "Collective dynamics of 'small-world' networks," *Nature*, vol. 393, no. 6684, pp. 440–442, June 1998.

[37] A. L. Barabasi and R. Albert, "Emergence of scaling in random networks," *Science (New York, N.Y.)*, vol. 286, no. 5439, pp. 509–512, 1999.

[38] R. Albert, I. Albert, and G. L. Nakarado, "Structural vulnerability of the north american power grid," *Phys. Rev. E*, vol. 69, p. 025103, Feb. 2004.

[39] M. Casals, "Topological complexity of the electricity transmission network. implications in the sustainability paradigm," Ph.D. dissertation, Universitat Politecnica de Catalunya, 2009.

[40] A. Fouad, Q. Zhou, and V. Vittal, "System vulnerability as a concept to assess power system dynamic security," *Power Systems, IEEE Transactions on*, vol. 9, no. 2, pp. 1009–1015, 1994.

[41] J. Salmeron, K. Wood, and R. Baldick, "Analysis of electric grid security under terrorist threat," *Power Systems, IEEE Transactions on*, vol. 19, no. 2, pp. 905–912, May 2004.

[42] G. Cai, K. Chan, W. Yuan, and G. Mu, "Identification of the vulnerable transmission segment and cluster of critical machines using line transient potential energy," *International Journal of Electrical Power & Energy Systems*, vol. 29, no. 3, pp. 199–207, 2007.

[43] J. Lu, Q. Ji, and Y. Zhu, "Power grid vulnerability assement based on energy function," in *Electric Utility Deregulation and Restructuring and Power Technologies (DRPT 2008)*, Nanjing, China, 2008, pp. 1039–1043, april 6–9.

[44] Q. Liu, J. Liu, and Q. Huang, "Configure vulnerability assessment based on potential energy model," in *International Conference on Sustainable Power Generation and Supply (SUPERGEN)*, Nanjing, China, 2009, pp. 1–7, april 6–7.

[45] A. J. Holmgren, "A framework for vulnerability assessment of electric power systems," in *Critical Infrastructure*, ser. Advances in Spatial Science, A. Murray and T. Grubesic, Eds. Springer Berlin Heidelberg, 2007, pp. 31–55.

[46] M. Shinozuka, X. Dong, T. C. Chen, and X. Jin, "Seismic performance of electric transmission network under component failures," *Earthquake Engineering & Structural Dynamics*, vol. 36, no. 2, pp. 227–244, 2007.

[47] P. Crucitti, V. Latora, and M. Marchiori, "A topological analysis of the italian electric power grid," *Physica A*, vol. 338, no. 1–2, pp. 92–97, 2004.

[48] R. Criado, J. Flores, B. Hernandez-Bermejo, J. Pello, and M. Romance, "Effective measurement of network vulnerability under random and intentional attacks," *Journal of Mathematical Modelling and Algorithms*, vol. 4, no. 3, pp. 307–316, 2005.

[49] J. E. Cotilla-Sanchez, "A complex network approach to analyzing the structure and dynamics of power grids," Ph.D. dissertation, The University of Vermont, 2009.

[50] C. Gomez, J. Buritica, M. Sanchez-Silva, and L. Duenas-Osorio, "Vulnerability assessment of infrastructure networks by using hierarchical decomposition methods," in *First International Conference on Vulnerability and Risk Analysis and Management (ICVRAM)*, Hyattsville, Maryland, 2011, april 11-13.

[51] E. Zio and L. Golea, "Analyzing the topological, electrical and reliability characteristics of a power transmission system for identifying its critical elements," *Reliability Engineering & System Safety*, vol. 101, no. 0, pp. 67–74, 2012.

[52] P. Hines, E. Cotilla-Sanchez, and S. Blumsack, "Do topological models provide good information about electricity infrastructure vulnerability?" *Chaos*, vol. 20, no. 3, p. 033122, 2010.

[53] T. Adachi and B. R. Ellingwood, "Comparative assessment of civil infrastructure network performance under probabilistic and scenario earthquakes," *Journal of Infrastructure Systems*, vol. 16, no. 1, pp. 1–10, 2010.

[54] R. K. McGuire, "Probabilistic seismic hazard analysis and design earthquakes: Closing the loop," *Bulletin of the Seismological Society of America*, vol. 85, no. 5, pp. 1275–1284, 1995.

[55] USGS, "Usgs national seismic hazard maps," U.S. Geological Survey, Tech. Rep., 2008, feb. 2013. [Online]. Available: http://earthquake.usgs.gov/hazards/products/conterminous/2008/

[56] FEMA, *Multi–hazard Loss Estimation Methodology: Earthquake model, $HAZUS^{MH}$ MR4*, Department of Homeland Security Emergency Preparedness and Response Directorate. Mitigation Division, Washington, D.C., 2003.

[57] *Minimum design loads for buildings and other structures*, ASCE 7-10, New York, 2010.

[58] S. E. Chang, M. Shinozuka, and J. E. M. II, "Probabilistic earthquake scenarios: Extending risk analysis methodologies to spatially distributed systems," *Earthquake Spectra*, vol. 16, no. 3, pp. 557–572, 2000.

[59] M. Shinozuka, X. Dong, X. Jin, and T. Cheng, "Seismic performance analysis for the ladwp power system," in *IEEE/PES Transmission Distrib. Conf. Exhibit. Asia Pac*, Dalian, China, 2005, aug. 15–17.

[60] C. Nuti, A. Rasulo, and I. Vanzi, "Seismic safety of network structures and infrastructures," *Structure and Infrastructure Engineering*, vol. 6, no. 1–2, pp. 95–110, 2010.

[61] B. T. Knight and L. Kempner, *Seismic Vulnerabilities and Retrofit of High-Voltage Electrical Substation Facilities*, 2009, ch. 56, pp. 1–12. [Online]. Available: http://ascelibrary.org/doi/abs/10.1061/41050%28357%2922

[62] T. Adachi and B. R. Ellingwood, "Serviceability assessment of electrical power transmission systems under probabilistically stated seismic hazards: case study for shelby county, tennessee," *Structure and Infrastructure Engineering*, vol. 5, no. 5, pp. 343–353, 2009.

[63] H. Jun and L. Jie, "Seismic reliability analysis of large electric power systems," *Earthquake Engineering and Engineering Vibration*, vol. 3, pp. 51–55, 2004.

[64] G. Gardini, R. Fregonese, M. E. Gobbi, E. Bon, and R. Calisti, "Probabilistic assessment of electric power grids vulnerability under seismic action: a case study," *Structure and Infrastructure Engineering*, pp. 1–20, 2012. [Online]. Available: http://www.tandfonline.com/doi/abs/10.1080/15732479.2011.653977

[65] L. Duenas-Osorio, J. I. Craig, and B. J. Goodno, "Seismic response of critical interdependent networks," *Earthquake Engineering & Structural Dynamics*, vol. 36, no. 2, pp. 285–306, 2007.

[66] H. Matt and A. Filiatrault, "Seismic response of high voltage transformers," in *Proceedings of the 6th U.S. Conference and Workshop on Lifeline Earthquake Engineering*, Long Beach, California, U.S.A., 2003, pp. 650–656.

[67] J. Dastous and A. Filiatrault, "Seismic displacement at interconnection points of substation equipment," in *Proceedings of the 6th U.S. Conference and Workshop on Lifeline Earthquake Engineering*, Long Beach, California, U.S.A., 2003, pp. 597–606.

[68] A. Schiff and L. Kempner, "Issues and guidance for institute of electrical and electronics engineers (ieee) 693 equipment qualification tests," in *Proceedings of the 6th U.S. Conference and Workshop on Lifeline Earthquake Engineering*, Long Beach, California, U.S.A., 2003, pp. 650–656.

[69] K. Pitilakis, "D3.3 - fragility functions for electric power system elements," SYNER-G, Tech. Rep., 2010.

[70] T. Anagnos, "Development of an electrical substation equipment performance database for evaluation of equipment fragilities," Department of Civil and Environmental Engineering, San Jose Sate University, Tech. Rep., Apr. 1999.

[71] I. Vanzi, "Structural upgrading strategy for electric power networks under seismic action," *Earthquake Engineering & Structural Dynamics*, vol. 29, no. 7, pp. 1053–1073, 2000.

[72] A.-S. Ang, J. Pires, and R. Villaverde, "A model for the seismic reliability assessment of electric power transmission systems," *Reliability Engineering & System Safety*, vol. 51, no. 1, pp. 7–22, 1996.

[73] I. Vanzi, "Seismic reliability of electric power networks: methodology and application," *Structural Safety*, no. 4, pp. 311–327, 1996.

[74] A. Rasulo, A. Goretti, and C. Nuti, "Performance of lifelines during the 2002 molise, italy, earthquake," *Earthquake Spectra*, vol. 65, no. 3, pp. 213–227, 2004.

[75] C. Nuti and I. Vanzi, "Earthquake structural retrofitting of electric power networks under economic constraints," in *Probabilistic Methods Applied to Power Systems, 2004 International Conference on*, 2004, pp. 987–992, sept 16.

[76] H. He and J. Guo, "Seismic disaster risk evaluation for power systems considering common cause failure," in *Zhongguo Dianji Gongcheng Xuebao/Proceedings of the Chinese Society of Electrical Engineering*, vol. 32, no. 28, 2012, pp. 44–54.

[77] F. Cavalieri, P. Franchin, P. Gehl, and B. Khazai, "Quantitative assessment of social losses based on physical damage and interaction with infrastructural systems," *Earthquake Engineering & Structural Dynamics*, vol. 41, no. 11, pp. 1569–1589, 2012.

[78] J. Pires, A.-S. Ang, and R. Villaverde, "Seismic reliability of electrical power transmission systems," *Nuclear Engineering and Design*, vol. 160, pp. 427–439, 1996.

[79] F. Capra, *The Web of Life: A New Synthesis of Mind and Matter*. Flamingo, London, 1997.

[80] J. Mingers and L. White, "A review of the recent contribution of systems thinking to operational research and management science," *European Journal of Operational Research*, vol. 207, no. 3, pp. 1147–1161, 2010.

[81] C. Gomez, M. Sanchez-Silva, L. Duenas-Osorio, and D. Rosowsky, "Hierarchical infrastructure network representation methods for risk-based decision-making," *Structure and Infrastructure Engineering*, pp. 1–15, 2010. [Online]. Available: http://www.tandfonline.com/doi/pdf/10.1080/15732479.2010.546415

[82] S. L. Everitt, Brian S. and M. Leese, *Cluster analysis*, 4th ed. London: Edward Arnold Publishers Ltd, 2001.

[83] J. A. Hartigan, *Clustering algorithms*. New York: John Wiley & Sons, 1975.

[84] R. Kolisch, "Resource allocation capabilities of commercial project management software packages," *Interfaces*, vol. 29, no. 4, pp. 19–31, 1999.

[85] C. Gomez, J. Buritica, M. Sanchez-Silva, and L. Duenas-Osorio, "Optimisation-based decision-making for complex networks in disastrous events," *International Journal of Risk Assessment and Management*, vol. 15, no. 5-6, 2011.

[86] F. Marle and L.-A. Vidal, "Project risk management processes: improving coordination using a clustering approach," *Research in Engineering Design*, vol. 22, pp. 189–206, 2011.

[87] J. Abonyi and B. Feil, *Cluster analysis for data mining and system Identification*. Boston: Birkhäuser, 2007.

[88] F. Aurenhammer, "Voronoi diagramsa survey of a fundamental geometric data structure," *ACM Comput. Surv.*, vol. 23, no. 3, pp. 345–405, Sep. 1991.

[89] R. Xu and D. Wunsch, "Survey of clustering algorithms," *Neural Networks, IEEE Transactions on*, vol. 16, no. 3, pp. 645–678, 2005.

[90] M. Filippone, F. Camastra, F. Masulli, and S. Rovetta, "A survey of kernel and spectral methods for clustering," *Pattern Recognition*, vol. 41, no. 1, pp. 176–190, 2008.

[91] A. K. Jain, M. N. Murty, and P. J. Flynn, "Data clustering: a review," *ACM Comput. Surv.*, vol. 31, no. 3, pp. 264–323, Sep. 1999.

[92] J. H. Ward, "Hierarchical grouping to optimize an objective function," *Journal of the American Statistical Association*, vol. 58, no. 301, pp. 236–244, 1963.

[93] P. H. A. Sneath and R. R. Sokal, *Numerical taxonomy: the principles and practice of numerical classification*. San Francisco, USA: Freeman, 1973.

[94] R. Kannan, S. Vempala, and A. Vetta, "On clusterings: good, bad, and spectral," in *41st Annual Symposium on the Foundation of Coputer Science*, S. Spring, Ed. IEEE Computer Society, November 2000, pp. 367–380.

[95] U. von Luxburg, M. Belkin, and O. Bousquet, "Consistency of spectral clustering," *Annals of Statistics*, vol. 36, no. 2, pp. 555–586, 2008.

[96] U. von Luxburg, O. Bousquet, and M. Belkin, "Limits of spectral clustering," in *Advances in Neural Information Processing Systems (NIPS)*, L. B. L.K. Saul, Y.Weiss, Ed., vol. 17. MIT Press, 2004, pp. 857–864.

[97] C. Gomez, M. Sanchez-Silva, and L. Duenas-Osorio, *Applications of Statistics and Probability in Civil Engineering*. Taylor % Francis Group, 2011, ch. Chapter 169. Clustering methods for risk assessment of infrastructure network systems, pp. 1389–1397.

[98] J. Shi and J. Malik, "Normalized cuts and image segmentation," *Pattern Analysis and Machine Intelligence, IEEE Transactions on*, vol. 22, no. 8, pp. 888–905, Aug. 2000.

[99] J. A. Buritica, M. Sanchez-Silva, and S. Tesfamariam, "A hierarchical-based approach to seismic vulnerability assessment of power transmission systems," 2012, submitted for publication.

[100] B. Gutenberg and C. F. Richter, "Frequency of earthquakes in california," *Bulletin of the Seismological Society of America*, vol. 34, no. 4, 1944.

[101] M. Sanchez-Silva and R. Rackwitz, "Socioeconomic implications of life quality index in design of optimum structures to withstand earthquakes," *Journal of Structural Engineering*, vol. 130, no. 6, pp. 969–977, 2004.

[102] K. W. Campbell and Y. Bozorgnia, "Updated near-source ground-motion (attenuation) relations for the horizontal and vertical components of peak ground acceleration and acceleration response spectra," *Bulletin of the Seismological Society of America*, vol. 93, no. 1, pp. 314–331, 2003.

[103] T. Nishimura and M. Horike, "The attenuation relationships of peak ground accelerations for the horizontal and the vertical components inferred from kyoshin network data," *Journal of Structural and Construction Engineering (Transactions of AIJ)*, no. 571, pp. 63–70, 2003.

[104] S. Ohno, K. Takahashi, and M. Motosaka, "Empirical estimation of horizontal and vertical motions based on california earthquake records and its application to japan inland earthquakes," *Journal of Structural and Construction Engineering (Transactions of AIJ)*, no. 544, pp. 39–46, 2001.

[105] T. Takahashi, S. Kobayashi, Y. Fukushima, J. X. Zhao, H. Nakamura, and P. G. Somerville, "A spectral attenuation model for japan using strong ground motion data base," in *Proceedings of 6th International Conference on Seismic Zonation*, 2000.

[106] H. Si and S. Midorikawa, "Attenuation relations for peak ground acceleration and velocity considering effects of fault type and site condition," *Journal of Structural and Construction Engineering (Transactions of AIJ)*, no. 523, pp. 63–70, 1999.

[107] N. Ambraseys, K. Simpson, and J. Bommer, "Prediction of horizontal response spectra in europe," *Earthquake Engineering and Structural Dynamics*, vol. 25, no. 4, pp. 371–400, 1996.

[108] W. B. Joyner and D. M. Boore, "Peak horizontal acceleration and velocity from strong motion records including records from the 1979 imperial valley, california earthquake," *Bulletin of the Seismological Society of America*, vol. 71, no. 6, pp. 2011–2038, Dec. 1981.

[109] J. B. Mander, "Fragility curve development for assessing the seismic vulnerability of highway bridges," in *The Earthquake Engineering Online Archive (NISEE e-Library)*. University at Buffalo, State University of New York, 1998, pp. 1–10.

[110] T. Anagnos and D. K. Ostrom, "Electrical substation equipment damage database for updating fragility estimates," in *12th World Conference on Earthquake Engineering (12WCEE)*, no. 2262, Auckland, N.Z., Jan-Feb 2000.

[111] G. Liu, C.-W. Liu, and Y. Yang, "Montecarlo simulation for seismic response analysis of electric power system in taiwan," NCREE/JRC joint workshop, 2003, taipei, Taiwan.

[112] H. Hwang and J. Huo, "Seismic fragiliy analysis of electric substation equipment and structures," *Probabilistic Engineering Mechanics*, vol. 13, no. 2, pp. 107–116, 1998.

[113] I. Vanzi, A. Rasulo, and S. Sigismondo, "Valutazione della sicurezza al sisma del sistema reti elettriche e procedura di adeguamiento: fase b, fragilita dei componenti," Dipartimento di Progetazione, Riabilitazione e Controllo delle Strutture, University G. D'Annuzio Of Chietiand Pescara, Italy, Tech. Rep., 2004, for Pricos-Cesi S.p.A., contract (U0950).

[114] H. H. Hwang and J.-R. Huo, "Seismic fragility analysis of electric substation equipment and structures," *Probabilistic Engineering Mechanics*, vol. 13, no. 2, pp. 107–116, 1998.

[115] D. Straub and A. D. Kiureghian, "Improved seismic fragility modeling from empirical data," *Structural Safety*, vol. 30, no. 4, pp. 320–336, 2008.

[116] S. Giovinazzi and A. King, "Estimating seismic impacts on lifelines: an international review for riskscape," in *New Zealand Society of Earthquake Engineering Annual Conference (NZSEE)*. Christchurch, New Zealand: University of Canterbury. Civil and Natural Resources Engineering, Apr. 2009.

[117] S. Blumsack, L. B. Lave, and M. Ilic, "A quantitative analysis of the relationship between congestion and reliability in electric power networks," *The Energy Journal*, vol. 0, no. 4, pp. 73–100, 2007.

[118] S. Van Dongen, "Graph clustering by flow simulation," Ph.D. dissertation, University of Utrecht, 2000.

[119] W. A. Hendricks and K. W. Robey, "The sampling distribution of the coefficient of variation," *The Annals of Mathematical Statistics*, vol. 7, no. 3, pp. 129–32, 1936.

[120] C. A. Cornell, "Engineering seismic risk analysis," *Bulletin of Seismological Society of America*, vol. 58, no. 5, pp. 1583–1606, 1968.

[121] F. Cavalieri, P. Franchin, J. A. Buritica, and S. Tesfamariam, "Models for seismic vulnerability analysis of power networks: comparative assessment," 2013, submitted for publication.

[122] P. Franchin and F. Cavalieri, "Seismic vulnerability of a complex interconnected infrastructure," in *Handbook of seismic risk analysis and management of civil infrastructure systems*, T. S. and G. K., Eds. Cambridge, UK: Woodhead Publishing Limited, 2013.

[123] NIAC, "A framework for establishing critical infrastructure resilience goals," National Infrastructure Advisory Council, Tech. Rep., 2010.

[124] G. Augusti and M. Ciampoli, "Multi-objective optimal allocation of resources to increase the seismic reliability of highways," *Mathematical Methods of Operations Research*, vol. 47, no. 1, pp. 131–164, 1998.

[125] Y. Fan, C. Liu, R. Lee, and A. S. Kiremidjian, "Highway network retrofit under seismic hazard," *Journal of Infrastructure Systems*, vol. 16, no. 3, pp. 181–187, 2010.

[126] F. Carturan, C. Pellegrino, C. Modena, R. Rossi, and M. Gastaldi, "Optimal resource allocation for seismic retrofitting of bridges in transportation networks," in *5th International Conference on Bridge Maintenance, Safety and Management*, 2010, pp. 1188–1195, july 11-15.

[127] L. Chang, F. Peng, Y. Ouyang, A. S. Elnashai, and B. F. Spencer, "Bridge seismic retrofit program planning to maximize postearthquake transportation network capacity," *Journal of Infrastructure Systems*, vol. 18, pp. 75–88, 2012.

[128] IEEE-693, "693-2005 ieee recommended practice for seismic design of substations," IEEE Power & Energy Society, Tech. Rep., 2005. [Online]. Available: http://standards.ieee.org/findstds/standard/693-2005.html

[129] M. Hosseini, A. Raoufi, A. H. Khalvati, and A. Soroor, "A seismic risk management model for electric power distribution networks in large cities by concentration on low-voltage substations," in *TCLEE 2009: Lifeline Earthquake Engineering in a Multihazard Environment*, Oakland, CA, 2009, pp. 252–261, june 28 - July 1.

[130] M. Caramia and P. Dell'Olmo, *Multi-objective Management in Freight Logistics Increasing Capacity, Service level and Saftey with Optimization Algorithms.* Springer, 2008, ch. Multi-objective Optimization.

[131] P. Berkhin, "A survey of clustering data mining techniques," in *Grouping Multidimensional Data*, J. Kogan, C. Nicholas, and M. Teboulle, Eds. Springer Berlin Heidelberg, 2006, pp. 25–71.

[132] D. Verma and M. Meila, "A comparison of spectral clustering algorithms," Department of CSE University of Washington, Tech. Rep. 98195-2350, 2003, seattle, WA.

[133] M. Meila and J. Shi, "Learning segmentation by random walks," in *In Advances in Neural Information Processing Systems.* MIT Press, 2000, pp. 470–477.

[134] A. Y. Ng, M. I. Jordan, and Y. Weiss, "On spectral clustering: Analysis and an algorithm," in *Advances In Neural Information Processing Systems.* MIT Press, 2001, pp. 849–856.

[135] A. Barabasi, *Linked: the new science of networks.* Cambridge, MA: Perseus Publishing, 2002.

[136] P. Crucitti, V. Latora, and M. Marchiori, "Model for cascading failures in complex networks," *Phys. Rev. E*, vol. 69, p. 045104, Apr 2004.

[137] J.-W. Wang and L.-L. Rong, "Cascade-based attack vulnerability on the us power grid," *Safety Science*, vol. 47, no. 10, pp. 133–1336, 2009.

[138] L. Duenas-Osorio and S. M. Vemuru, "Cascading failures in complex infrastructure systems," *Structural Safety*, vol. 31, no. 2, pp. 157–167, 2009. [Online]. Available: http://www.sciencedirect.com/science/article/pii/S016747300800057X

[139] I. Hernandez-Fajardo and L. Duenas-Osorio, *Probabilistic Study of Cascading Failures in Complex Interdependent Lifeline Systems*, ch. 25, pp. 205–213. [Online]. Available: http://ascelibrary.org/doi/abs/10.1061/41170%28400%2925

Appendix A

IEEE-14 Test Case

Table A.1: Branch data of IEEE-14 Test Case

Tap bus number (I)	Z bus number (I)	Branch reactance (X)
1	2	0.05917
1	5	0.22304
2	3	0.19797
2	4	0.17632
2	5	0.17388
3	4	0.17103
4	5	0.04211
4	7	0.20912
4	9	0.55618
5	6	0.25202
6	11	0.1989
6	12	0.25581
6	13	0.13027
7	8	0.17615
7	9	0.11001
9	10	0.0845
9	14	0.27038
10	11	0.19207
12	13	0.19988
13	14	0.34802

Table A.2: Electrical distance matrix of IEEE-14 Test Case

0	0.149	0.095	0.087	0.248	0.224	0.4	0.234	0.279	0.314	0.374	0.312	0.366
0.149	0	0.106	0.123	0.276	0.239	0.416	0.251	0.299	0.337	0.401	0.338	0.387
0.095	0.106	0	0.034	0.181	0.136	0.313	0.15	0.198	0.24	0.305	0.242	0.288
0.087	0.123	0.034	0	0.17	0.158	0.334	0.165	0.209	0.24	0.296	0.235	0.293
0.248	0.276	0.181	0.17	0	0.219	0.395	0.181	0.192	0.147	0.141	0.091	0.239
0.224	0.239	0.136	0.158	0.219	0	0.176	0.09	0.156	0.237	0.335	0.266	0.265
0.4	0.416	0.313	0.334	0.395	0.176	0	0.266	0.332	0.413	0.512	0.442	0.441
0.234	0.251	0.15	0.165	0.181	0.09	0.266	0	0.075	0.177	0.293	0.221	0.194
0.279	0.299	0.198	0.209	0.192	0.156	0.332	0.075	0	0.144	0.309	0.24	0.245
0.314	0.337	0.24	0.24	0.147	0.237	0.413	0.177	0.144	0	0.276	0.217	0.292
0.374	0.401	0.305	0.296	0.141	0.335	0.512	0.293	0.309	0.276	0	0.13	0.319
0.312	0.338	0.242	0.235	0.091	0.266	0.442	0.221	0.24	0.217	0.13	0	0.222
0.366	0.387	0.288	0.293	0.239	0.265	0.441	0.194	0.245	0.292	0.319	0.222	0

Appendix B

IEEE-118 Test Case

Table B.1: Metrics and ranking for IEEE-118 network - 1

Node ID	D	$Rank_D$	B	$Rank_B$	T	$Rank_T$	W	$Rank_W$
S-1	2	56	2.21E-04	90	5.30E+01	74	7.14E-03	102
S-2	2	57	0.00E+00	92	3.18E+01	98	7.87E-03	99
S-3	3	37	2.67E-02	67	8.52E+01	52	1.14E-02	79
S-4	5	11	2.24E-01	29	3.79E+02	7	3.88E-03	113
S-5	2	60	1.40E-03	85	4.23E+01	84	1.54E-02	67
S-6	2	61	2.87E-02	65	4.75E+02	3	4.24E-03	111
S-7	4	22	8.06E-02	43	1.63E+02	27	1.35E-02	72
S-8	2	62	0.00E+00	95	3.75E+01	91	1.19E-02	76
S-9	2	63	4.05E-03	80	1.98E+01	111	1.88E-02	54
S-10	2	64	0.00E+00	96	2.73E+01	101	1.69E-02	60
S-11	6	5	4.81E-01	16	2.60E+02	17	2.78E-02	31
S-12	2	66	2.32E-02	73	3.75E+01	92	2.90E-02	28
S-13	2	67	2.95E-04	88	5.28E+01	75	3.09E-02	24
S-14	2	68	2.28E-03	83	6.19E+01	68	3.20E-02	22
S-15	4	24	5.16E-02	51	1.74E+02	25	2.76E-02	32
S-16	2	70	0.00E+00	98	4.05E+01	88	9.80E-03	85
S-17	2	71	1.96E-04	91	2.82E+01	100	9.84E-03	84
S-18	4	26	5.60E-01	13	3.33E+02	10	2.89E-02	29
S-19	2	72	0.00E+00	99	2.57E+01	103	2.68E-02	33
S-20	2	73	0.00E+00	100	3.62E+01	93	3.69E-02	14
S-21	6	6	2.43E-01	27	2.74E+02	16	1.41E-02	69
S-22	3	42	7.05E-01	12	2.87E+02	15	3.80E-02	12
S-23	2	75	0.00E+00	101	6.34E+01	67	1.86E-02	55
S-24	2	76	0.00E+00	102	4.15E+01	85	8.79E-03	91
S-25	2	77	4.05E-03	81	2.09E+01	110	3.60E-02	17
S-26	2	78	5.89E-04	87	4.11E+01	87	4.02E-02	11
S-27	3	44	2.38E-02	72	9.83E+01	44	4.64E-02	8
S-28	3	46	2.39E-02	71	7.35E+01	59	1.00E-01	1
S-29	2	79	0.00E+00	104	4.00E+01	89	2.95E-02	26
S-30	2	80	0.00E+00	105	5.43E+01	72	2.36E-02	37
S-31	3	47	3.58E-02	62	6.80E+01	64	3.28E-02	20
S-32	2	81	2.95E-04	89	3.27E+01	96	2.10E-02	46
S-33	2	82	0.00E+00	106	2.68E+01	102	7.40E-03	101
S-34	2	83	0.00E+00	108	3.79E+01	90	8.41E-03	94
S-35	2	84	2.33E-03	82	2.14E+01	109	7.99E-03	97
S-36	3	49	0.00E+00	109	1.42E+02	32	1.17E-02	77
S-37	2	85	1.10E-01	35	1.77E+02	24	9.26E-03	87
S-38	3	50	1.99E-01	32	2.13E+02	21	1.08E-02	80
S-39	2	86	0.00E+00	110	5.20E+01	76	3.21E-02	21

Table B.2: Metrics and ranking for IEEE-118 network - 2

Node ID	D	$Rank_D$	B	$Rank_B$	T	$Rank_T$	W	$Rank_W$
S-40	4	33	1.27E+00	6	2.12E+02	22	3.74E-02	13
S-41	3	51	4.54E-02	54	2.42E+01	105	2.33E-02	39
S-42	5	17	3.27E-01	23	1.54E+02	29	4.95E-02	7
S-43	2	90	8.57E-02	41	7.30E+01	60	5.50E-02	6
S-44	2	91	8.66E-02	40	6.36E+01	66	2.18E-02	43
S-45	2	92	9.86E-01	8	5.45E+01	70	2.19E-02	42
S-46	3	53	3.61E-01	21	9.36E+01	48	4.16E-02	10
S-47	2	93	4.18E-02	58	4.87E+01	78	2.57E-02	35
S-48	2	94	5.60E-02	48	2.48E+01	104	3.06E-02	25
S-49	2	95	4.58E-02	53	1.14E+02	38	6.64E-02	4
S-50	2	98	2.60E-02	68	7.10E+01	62	9.31E-03	86
S-51	5	19	9.87E-01	7	1.24E+02	34	7.61E-02	3
S-52	2	99	5.38E-02	49	4.47E+01	81	1.58E-02	64
S-53	5	20	1.30E+00	5	5.62E+01	69	1.68E-02	61
S-54	2	100	1.51E-01	33	2.31E+01	107	1.84E-02	56
S-55	2	101	4.31E-01	17	3.59E+01	94	4.59E-02	9
S-56	2	103	5.84E-02	46	4.80E+01	79	1.91E-02	52
S-57	2	104	3.23E-02	64	5.37E+01	73	2.01E-02	50
S-58	3	55	2.27E-01	28	7.65E+01	55	2.04E-02	49
S-59	2	106	5.20E-02	50	3.39E+01	95	5.20E-03	106
S-60	2	107	2.58E-02	69	3.13E+01	95	3.40E-03	115
S-61	2	109	1.05E-01	36	1.11E+01	99	1.77E-02	57
S-62	2	110	7.72E-02	44	2.40E+01	114	1.34E-02	73
S-63	1	118	0.00E+00	118	2.19E+01	106	1.74E-02	58
S-64	2	111	2.75E-02	66	4.12E+01	108	2.17E-02	44
G-1	2	58	0.00E+00	93	1.13E+02	86	4.82E-03	108
G-2	2	59	2.45E-02	70	1.01E+02	41	8.59E-03	92
G-3	3	38	2.92E-01	26	4.75E+02	4	8.17E-03	96
G-4	1	112	0.00E+00	94	4.71E+02	5	2.87E-03	117
G-5	7	3	1.18E-01	34	8.84E+01	49	5.00E-03	107
G-6	5	12	6.14E-02	45	1.19E+02	37	1.28E-02	74
G-7	2	65	0.00E+00	97	8.75E+01	50	1.01E-02	83
G-8	4	23	5.76E-02	47	4.57E+01	80	1.66E-02	62
G-9	3	39	1.38E-02	76	1.36E+01	112	2.94E-02	27
G-10	3	40	1.40E-03	86	3.28E+02	11	7.87E-03	98
G-11	2	69	1.30E-02	77	3.47E+02	8	7.10E-03	103
G-12	4	25	3.24E-02	63	1.54E+02	28	8.92E-03	89
G-13	3	41	2.31E-02	74	5.43E+01	71	1.03E-02	82
G-14	5	13	3.87E-01	19	1.22E+02	35	1.14E-02	78
G-15	4	27	1.04E-01	37	1.00E+02	43	2.11E-02	45
G-16	2	74	2.08E-03	84	3.21E+01	97	2.65E-02	34

Table B.3: Metrics and ranking for IEEE-118 network - 3

Node ID	D	$Rank_D$	B	$Rank_B$	T	$Rank_T$	W	$Rank_W$
G-17	4	28	3.75E-02	61	1.01E+02	42	1.55E-02	66
G-18	3	43	5.56E-03	78	7.68E+01	53	1.62E-02	63
G-19	3	45	0.00E+00	103	5.05E+01	77	6.19E-02	5
G-20	9	1	2.19E-01	30	3.42E+02	9	2.32E-02	40
G-21	5	14	4.99E-02	52	7.52E+01	56	8.27E-03	95
G-22	3	48	0.00E+00	107	7.41E+01	58	1.06E-02	81
G-23	5	15	4.24E-02	56	8.66E+01	51	6.22E-03	104
G-24	6	7	9.43E-02	38	2.90E+02	13	6.00E-03	105
G-25	4	29	4.50E-02	55	2.27E+02	20	1.95E-02	51
G-26	4	30	4.14E-03	79	9.37E+01	47	2.36E-02	38
G-27	4	31	7.43E-01	9	4.47E+02	6	2.05E-02	48
G-28	4	32	8.18E-02	42	2.32E+02	19	1.89E-02	53
G-29	6	8	2.13E-01	31	5.53E+02	1	2.90E-03	118
G-30	5	16	8.80E-02	39	1.22E+02	36	9.96E-02	2
G-31	2	87	0.00E+00	111	1.30E+01	113	3.32E-02	18
G-32	1	113	0.00E+00	112	9.25E+00	116	3.12E-02	23
G-33	2	88	0.00E+00	113	7.68E+01	54	2.09E-02	47
G-34	2	89	4.21E-02	57	7.24E+01	61	3.65E-02	15
G-35	6	9	3.03E+00	3	1.70E+02	26	1.73E-02	59
G-36	7	4	6.76E+00	1	2.89E+02	14	9.17E-03	88
G-37	3	52	7.30E-01	10	7.46E+01	57	2.89E-02	30
G-38	5	18	7.29E-01	11	1.44E+02	31	3.62E-02	16
G-39	1	114	0.00E+00	114	2.51E+00	118	8.82E-03	90
G-40	4	34	3.48E-01	22	4.98E+02	2	8.47E-03	93
G-41	2	96	1.82E-02	75	6.86E+01	63	1.23E-02	75
G-42	2	97	3.85E-02	59	7.70E+00	117	4.62E-03	109
G-43	6	10	1.39E+00	4	2.37E+02	18	4.06E-03	112
G-44	2	102	2.93E-01	25	4.30E+01	83	1.42E-02	68
G-45	8	2	5.86E+00	2	2.98E+02	12	3.87E-03	114
G-46	4	35	5.54E-01	14	1.52E+02	30	1.57E-02	65
G-47	3	54	4.25E-01	18	9.69E+01	45	4.31E-03	110
G-48	5	21	4.95E-01	15	1.07E+02	40	3.31E-02	19
G-49	2	105	3.83E-02	60	6.37E+01	65	3.24E-03	116
G-50	4	36	2.99E-01	24	1.36E+02	33	1.39E-02	70
G-51	1	115	0.00E+00	115	4.37E+01	82	1.39E-02	71
G-52	1	116	0.00E+00	116	9.69E+01	46	2.28E-02	41
G-53	2	108	3.73E-01	20	1.04E+01	115	7.63E-03	100
G-54	1	117	0.00E+00	117	2.12E+02	23	2.44E-02	36